Dislocation-density dynamics for modeling the cores and Peierls stress of curved dislocations

Yuqi Zhang and Alfonso H.W. Ngan*

Department of Mechanical Engineering, The University of Hong Kong, Pokfulam Road,

Hong Kong, P.R. China

*Author to whom correspondence should be addressed. E-Mail: hwngan@hku.hk. Tel: +852 3917 7900.

Abstract:

Although continuum dislocation models can describe dislocation cores, they are generally incapable of describing the Peierls stress, due to the invariance of the misfit energy and a lack of means to trigger configurational changes in the dislocation core as the dislocation moves. In this work, a dislocation-density dynamics framework for modeling dislocations at an "intensive" resolution scale finer than the dislocation core is established. In this approach, the inter-dislocation elastic interaction is accounted for via Mura's formula after singularity removal, and the interaction within the dislocation core is modelled by introducing a phenomenological formalism of the lattice misfit stress to balance the elastic interaction between dislocation contents, leading to not only a stable width of the dislocation as it travels, but also the expected Peierls stress. This framework is implemented numerically by using a divergence-preserving finite-volume method for curved dislocations gliding on 2D slip planes in general. Simulation examples of various dislocation mechanisms, including shrinkage and expansion of dislocation loops, the Frank-Read source, and Orowan looping, are given. The simulated results exhibit excellent preservation of continuity of dislocation densities during their evolution, while the detailed core structures and Peierls stress are clearly elucidated.

Keywords: Dislocation dynamics; dislocation density; dislocation core; Peierls stress; crystal plasticity.

1. Introduction

Although glissile dislocations are associated with the collective displacements of atoms corresponding to the relative slip of crystallographic planes, they are often described as topological defects under different levels of coarse graining (LeSar, 2014). Dislocation models may focus on three increasing levels of resolution that are more coarse-grained than atomic (i.e. molecular dynamics), namely, (i) extensive, (ii) discrete, and (iii) intensive (Ngan, 2017). As shown in Fig. 1, "extensive" dislocation models are highly coarse-grained models based on a pixel length scale that is significantly larger than the mean spacing between dislocations, so that individual dislocations are not resolved, but are represented as a smeared out dislocation density. On the next level, "discrete" dislocation models treat dislocations as individual curvilinear objects without elucidation of their cores, which may nevertheless control the glide, cross-slip or climb mobility of the dislocation. On a finer level, "intensive" models are based on a length scale which, although is still larger than atomic, is smaller than the dislocation core width, so that core phenomena such as dissociation into partial dislocations or non-planar spreading can be modeled. In both extensive and intensive models, dislocation contents are depicted as a spatial density function that evolves temporally (Acharya et al., 2006; Acharya and Roy, 2006; Arsenlis et al., 2004; Arsenlis and Parks, 2002; Engels et al., 2012; Gbemou et al., 2016; Groma et al., 2016, 2003, Hochrainer et al., 2014, 2007; Leung et al., 2015; Leung and Ngan, 2016; Li et al., 2014; Roy and Acharya, 2005; Sandfeld et al., 2015; Varadhan et al., 2006), albeit on very different space-resolution scales as mentioned above, and it may

also be argued that in discrete models, the curvilinear representation may still be regarded as a delta-function dislocation density that does not change shape as the dislocation moves.

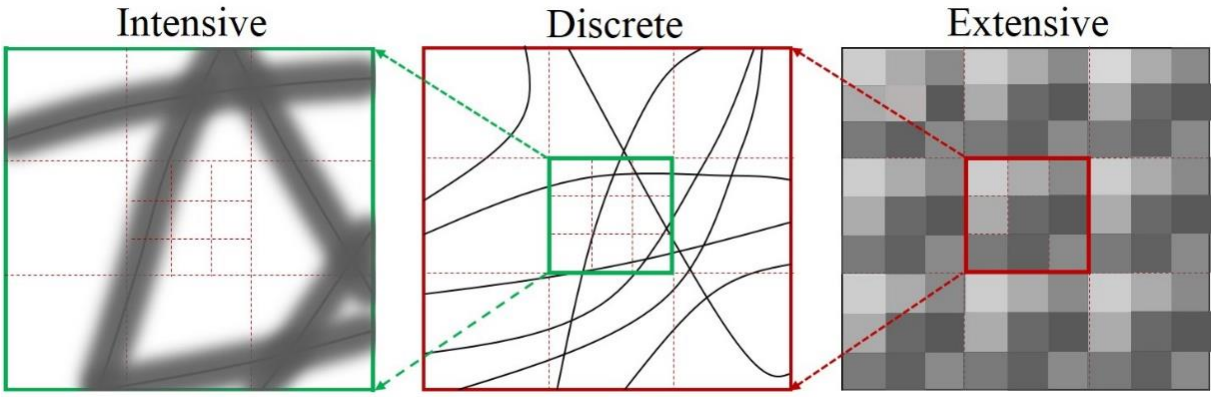

Fig. 1 The "intensive", "discrete" and "extensive" representations of dislocation microstructures.

As has been pointed out recently (Ngan, 2017), the three levels of representation of dislocations depicted in Fig. 1 require distinctive modeling strategies, from the representation of the dislocation density itself, to kinematics and dynamics. For a specific slip system, dislocation density can in general be represented as a field over spatial points $\mathbf{r}$ in two ways, namely, (i) a vector field $\boldsymbol{\rho}(\mathbf{r})$ for the net or geometrically-necessary-dislocation (GND) density, with the line length and direction of the net GND over a volume $dV(\mathbf{r})$ at $\mathbf{r}$ given as $\boldsymbol{\rho}(\mathbf{r})dV(\mathbf{r})$, and (ii) a scalar field $\varrho(\mathbf{r},\theta)$ for the density of all the dislocations over both space $\mathbf{r}$ and dislocation character θ, so that $\varrho(\mathbf{r},\theta)dV(\mathbf{r})d\theta$ gives the line length of dislocations with character from θ to $\theta + d\theta$ within a volume dV at $\mathbf{r}$. The well-known Nye tensor $\boldsymbol{\alpha} = \mathbf{b} \otimes \boldsymbol{\rho}$ is based on the vector representation $\boldsymbol{\rho}$ with information about the Burgers vector $\mathbf{b}$ incorporated (Nye, 1953), but for a specific slip system with a given $\mathbf{b}$, it suffices only to consider $\boldsymbol{\rho}$. In the "extensive" representation of dislocation microstructures, the GND density $\boldsymbol{\rho}$ obeys (Acharya et al., 2006; Acharya

and Roy, 2006; Gbemou et al., 2016; Hochrainer et al., 2014, 2007; Roy and Acharya, 2005; Varadhan et al., 2006):

$$\dot{\boldsymbol{\rho}} = -\boldsymbol{\nabla} \times (\boldsymbol{\rho} \times \mathbf{v}) \tag{1}$$

which is, in fact, a conservation law for general 3D curves moving in a 3D space with a velocity field **v** (Acharya et al., 2006; Acharya and Roy, 2006; Kröner, 1958; Mura, 2013; Roy and Acharya, 2005; Sandfeld et al., 2015; Varadhan et al., 2006). To incorporate the effects of the statistically stored dislocations (SSDs) which are not embodied in **ρ**, Acharya and Roy (Acharya et al., 2006; Acharya and Roy, 2006) introduced a flux of the SSDs into eqn. (1) but the evolution law for this SSD flux is not exactly known and can only be modelled phenomenologically. A continuum dislocation-density model for straight, parallel dislocations was also proposed (Groma et al., 2016, 2003), but curvilinear characteristics are missing in such a description. To completely specify the dislocation microstructure in the "extensive" picture, the "all-density" representation $\varrho(\mathbf{r}, \theta)$ mentioned above would be needed, and a simple kinematic law has recently been derived as (Ngan, 2017):

$$\dot{\varrho}(\mathbf{r}, \theta) = -\boldsymbol{\nabla}(\varrho v) \cdot \widehat{\boldsymbol{\theta}} - \frac{\partial(\varrho\omega)}{\partial\theta} \tag{2}$$

where $\boldsymbol{\nabla}$ is the gradient operator in the 2-D **r**-space of the slip plane, v and ω are the linear and rotational speed of the dislocations respectively, $\widehat{\boldsymbol{\theta}}$ is the positive circumferential direction of the dislocation character θ on the slip plane The two terms in eqn. (2) correspond to the approach of dislocations towards **r**, and tilting of the dislocations already situated at **r**, respectively. Hochrainer and co-workers (Hochrainer et al., 2014, 2007) have in fact proposed earlier on an alternative evolution law for ϱ which was shown to be equivalent to eqn. (2) (Ngan, 2017), but this involves the dislocation curvature as a second variable which has to be solved from another governing equation (Hochrainer et al., 2014, 2007; Sandfeld et al., 2015).

In the "discrete" picture of dislocation microstructure, the shape of the dislocation core does not change as the dislocation moves. Thus, instead of a general vector field $\boldsymbol{\rho}(\mathbf{r})$ for use in eqn. (1), a "discrete" dislocation I gliding on a slip plane is represented by the following density fields (Ngan, 2017):

$$\begin{cases} \boldsymbol{\rho}^I(\mathbf{r}) = \frac{\delta_r(r'^I)}{\mathrm{b}}\,\hat{\boldsymbol{\xi}}^I \\ \varrho^I(\mathbf{r},\theta) = \frac{\delta_r(r'^I)}{\mathrm{b}}\,\frac{\delta_\theta(\theta'^I)}{2\pi} \end{cases} \tag{3}$$

where $r'^I(\mathbf{r})$ is the shortest distance from a given field point $\mathbf{r}$ to the dislocation curve, $\hat{\boldsymbol{\xi}}^I$ and θ^I are, respectively, the unit line direction and angular character of the dislocation at the point closest to $\mathbf{r}$, $\theta'^I = \theta - \theta^I$, b is the atomic thickness of the slip plane, and δ_r and δ_θ are delta-like functions satisfying $\int_{-\infty}^{+\infty}\delta_r(r)dr = 1$, $\int_0^{2\pi}\delta_\theta(\theta)d\theta = 2\pi$. The kinematic laws for $\boldsymbol{\rho}^I$ and $\varrho^I(\mathbf{r},\theta)$ were shown to be (Ngan, 2017):

$$\begin{cases} \dot{\boldsymbol{\rho}}^I = -\frac{\partial \rho^I}{\partial r'^I} v^I \hat{\boldsymbol{\xi}}^I + \rho^I \dot{\hat{\boldsymbol{\xi}}}^I \\ \dot{\varrho}^I(\mathbf{r},\theta) = -v^I\,\frac{\partial \varrho^I}{\partial r'^I} - \omega^I\,\frac{\partial \delta\varrho^I}{\partial \theta'^I} \end{cases} \tag{4}$$

where v^I is the speed of approach of the dislocation I towards $\mathbf{r}$, ω^I is the rotational speed of the dislocation, and the two terms in each of the two equations above also correspond to the "approach" and "tilting" of the dislocation respectively. It should be noted that eqn. (2) for the overall "extensive" density $\varrho^I(\mathbf{r},\theta)$ is derivable from eqns. (4) by summing up the effects of the densities $\boldsymbol{\rho}^I$ or $\varrho^I(\mathbf{r},\theta)$ for all individual dislocations I that make up the overall density ϱ (Ngan, 2017).

For "intensive" dislocations gliding on their slip planes, eqn. (1) can be used to deduce a suitable kinematic law (Varadhan et al., 2006), subjected to certain caution which will be discussed in Section 2.1 below. In terms of dynamics, in the "extensive" picture mutual interactions of dislocations have to be modelled phenomenologically, such as using the Taylor hardening law of (density)$^{1/2}$, and the lattice

resistance to dislocation motion is modelled as a constant friction (Arsenlis et al., 2004; Arsenlis and Parks, 2002; Engels et al., 2012; Leung et al., 2015; Leung and Ngan, 2016; Li et al., 2014). In "discrete" or "intensive" models, however, the Taylor law of $(\text{density})^{1/2}$ is no longer valid as the spatial resolution of the density is on individual dislocation level or below, and specific strategies have to be developed to care for dislocation intersections (Bulatov et al., 2006). In "discrete" models, lattice friction is still treated as constant, but in "intensive" models, lattice friction should arise from a detailed consideration of the lattice disregistry in the dislocation core (Banerjee et al., 2007; Gbemou et al., 2016; Koslowski et al., 2002; Martínez et al., 2008; Wang et al., 2001; Xiang et al., 2008, 2003), as was done in the classical Peierls-Nabarro model for straight dislocations (Hirth and Lothe, 1982; Peierls, 1940).

The above summary shows that there can be no unified framework for density-field modeling of dislocations that can fit all levels of spatial resolution that are pertinent to dislocation plasticity. Most of the previous work on dislocation-density modeling focused on the "extensive" scale (Acharya et al., 2006; Acharya and Roy, 2006; Hochrainer et al., 2014, 2007; Roy and Acharya, 2005), and the "discrete" level is currently mainly handled by Discrete Dislocation Dynamics (DDD) which focuses on the evolution of nodal points on dislocations in a Lagrangian framework. Although the cores of dislocations control their glide, cross-slip or climb mobility, much less attention has been paid to develop dislocation-density models on this length scale, except the classical Peierls-Nabarro model which was in fact the first dislocation-density model, albeit for straight dislocations only. A group of previous work has attempted to model single dislocations using dislocation density (Gbemou et al., 2016; Leung and Ngan, 2016; Varadhan et al., 2006), but the treatment ignored dislocation interactions or dynamics (Varadhan et al., 2006), or was confined to one dimensional, straight dislocation cores (Gbemou et al., 2016), or the consideration of dislocation core lacks details of the lattice disregistry which is the very nature of lattice friction (Leung and Ngan, 2016). Previous *bona fide* "intensive" models for curved dislocations include

phase-field type models that involve plastic slip (Banerjee et al., 2007; Koslowski et al., 2002; Wang et al., 2001) or "level sets" (Xiang et al., 2008, 2003; Zhu et al., 2014) as variables, but their connection with the laws governing dislocation density is not completely transparent (Roy and Acharya, 2005), and lattice friction is again not described by these models. We also note in passing that specific partial dislocation dissociation dislocation has also been modeled within the framework of DDD (Martínez et al., 2008).

In the present study, we propose a new dislocation-density framework for the "intensive" description of dislocations. Compared with earlier phase-field models (Banerjee et al., 2007; Koslowski et al., 2002; Wang et al., 2001; Xiang et al., 2008, 2003), this framework makes use of the dislocation density as a variable which will connect it to previous literatures on dislocation-density approaches. To handle "intensive" dislocation cores, we aim at tackling two major problems: one is to incorporate core interactions that will allow the Peierls stress to naturally arise, and the other is to adapt a divergence-preserving numerical method to solve the evolution law for the dislocation density in order to ensure dislocation continuity. Numerical simulations of the glide motion of single dislocations on their 2D slip planes are presented.

2. Theory

2.1 Dynamics law for density of glissile, "intensive" dislocations on a specific slip system

For a given slip system with a specific Burgers vector, eqn. (1) implies that at any point **r** in space (or on the slip plane in the context of glissile dislocations), the dislocation content is represented completely by only one vector quantity $\boldsymbol{\rho}$. While we have seen that this is problematic for the "extensive" picture, we argue here that eqn. (1) is a good assumption in the "intensive" picture, provided that we ignore intersection points or nodes between dislocations. As mentioned in Section 1 above, since the pixel

resolution in the "intensive" picture is sub-dislocation, at any point **r** on the slip plane the dislocation content is either zero if no dislocation passes through that point, or that due to *one* particular dislocation if that point falls within the core of a given dislocation. For the latter case the line orientation of the passing dislocation can form the required direction of the vector **ρ** implied in eqn. (1), and so the vector field **ρ**(**r**) implied in eqn. (1) should be a meaningful quantity in the "intensive" picture. Here, we ignore dislocation nodes where more than one dislocation meet – such nodes are either immobile or the locations where dislocation reactions occur which would need special considerations, as in the case of discrete dislocation dynamics (Bulatov et al., 2006). Varadhan et al. (Varadhan et al., 2006) have indeed made use of eqn. (1) to model single dislocations on a slip plane without intersections.

Let us define formally the **ρ** in eqn. (1) for use in the "intensive" picture. Consider the parallel content in the core of a given dislocation with line direction $\hat{\boldsymbol{\xi}}$ on the slip plane, as shown in Fig. 2. The area density of dislocations is defined as $\rho = dN/dA$ where dN is the dislocation content threading a cross-sectional area dA of the slip plane perpendicular to $\hat{\boldsymbol{\xi}}$, as shown in Fig. 2. For cross-sectional areas $dA_e = dA/\xi_e$ and $dA_s = dA/\xi_s$ perpendicular to the edge and screw directions $\hat{\mathbf{x}}_e$ and $\hat{\mathbf{x}}_s$ respectively, the same dislocation content dN correspond to area densities $\rho_e = dN/dA_e = \rho\xi_e = \boldsymbol{\rho}\cdot\hat{\mathbf{x}}_e$ and $\rho_s = dN/dA_s = \boldsymbol{\rho}\cdot\hat{\mathbf{x}}_s$, so that we can write

$$\boldsymbol{\rho} = \frac{dN}{dA}\hat{\boldsymbol{\xi}} = \boldsymbol{\rho}_e + \boldsymbol{\rho}_s = \rho_e\hat{\mathbf{x}}_e + \rho_s\hat{\mathbf{x}}_s \tag{5}$$

where $\boldsymbol{\rho} = \rho\hat{\boldsymbol{\xi}}$ is the dislocation density vector and $\rho = \|\boldsymbol{\rho}\| = \sqrt{{\rho_e}^2 + {\rho_s}^2}$ is the magnitude of **ρ**.

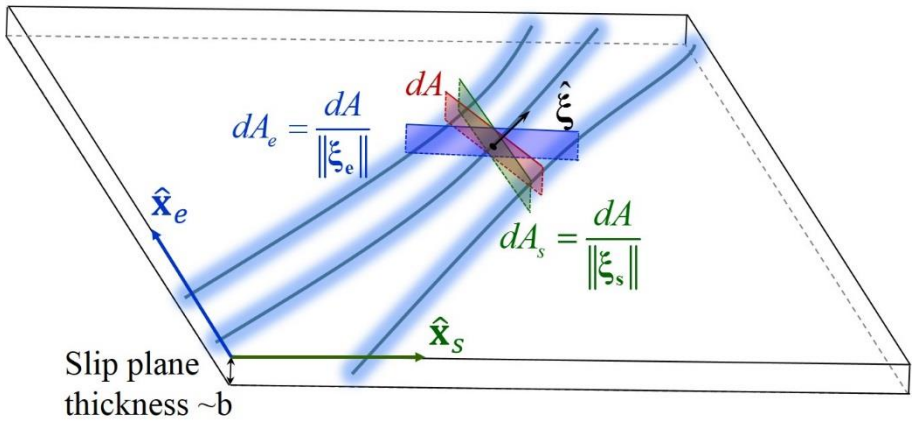

Fig. 2 Definition of dislocation density on a slip plane. dA is a small cross-sectional area of the slip plane (of thickness b) perpendicular to the dislocation line $\hat{\boldsymbol{\xi}}$.

The evolution law of $\boldsymbol{\rho}$ can now be obtained from eqn. (1), together with the condition that the velocity $\mathbf{v}$ for glissile dislocation contents must be lying on the slip plane in an orthogonal direction to the dislocation line $\hat{\boldsymbol{\xi}}$, i.e. $\mathbf{v} = v(\hat{\mathbf{n}} \times \hat{\boldsymbol{\xi}})$ where $\hat{\mathbf{n}}$ is the slip plane normal. Eqn. (1) then gives (Ngan, 2017; Varadhan et al., 2006):

$$\dot{\boldsymbol{\rho}} = \dot{\rho}_e \hat{\mathbf{x}}_e + \dot{\rho}_s \hat{\mathbf{x}}_s = -\frac{\partial(\rho v)}{\partial \mathbf{x}_e} \hat{\mathbf{x}}_s + \frac{\partial(\rho v)}{\partial \mathbf{x}_s} \hat{\mathbf{x}}_e \tag{6}$$

As in previous work (Engels et al., 2012; Leung and Ngan, 2016), in the rest of this paper, the velocity magnitude v is assumed to be governed by a power law of the effective glide stress τ^{eff}:

$$v = \text{sgn}(\tau^{\text{eff}}) v_0 \left| \tau^{\text{eff}} / \tau_0 \right|^m \tag{7}$$

where v_0, τ_0 and m are constants. The effective glide stress τ^{eff} is given by

$$\tau^{\text{eff}}(\mathbf{x}) = \tau^{\text{ext}}(\mathbf{x}) + \tau^{\text{dis}}(\mathbf{x}) \tag{8}$$

where $\tau^{\text{ext}}$is the stress from external loading and interaction with other microstructures such as second-phase precipitates, and τ^{dis} is the resolved shear stress due to mutual-dislocation interactions, arising from elastic interaction with other unit dislocations, and "self interactions" within the core of the same dislocation. In the following section, the interactive stresses will be discussed in detail.

2.2 Mutual dislocation interactions

2.2.1 Adapting Mura's formula for dislocation densities

Mura's formula (Mura, 2013) gives the stress field σ_{ij}^{I} induced by a dislocation loop L^I as:

$$\sigma_{ij}^{I}(\mathbf{x}) = C_{ijkl}\epsilon_{lnh}C_{pqmn}b_m^I \int_{L^I} G_{kp,q}(\mathbf{x}-\mathbf{x}')\xi_h(\mathbf{x}')dl(\mathbf{x}') \tag{9}$$

where C_{ijkl} is the elastic modulus, ϵ_{lnh} is the permutation tensor, G_{kp} are the Green's functions and $G_{kp,q} = \partial G_{kp}/\partial x_q$, x_q are coordinates of $\mathbf{x}$, b_m^I is the Burger's vector and ξ_h is the unit tangent vector on L^I. For an isotropic material, the elastic modulus and Green's functions are

$$C_{ijkl} = \lambda\delta_{ij}\delta_{kl} + \mu(\delta_{ik}\delta_{jl} + \delta_{il}\delta_{kj}) \tag{10}$$

$$G_{ij}(\mathbf{x}-\mathbf{x}') = \frac{1}{8\pi\mu}\left[\delta_{ij}\partial_p\partial_p R - \frac{1}{2(1-\nu)}\partial_i\partial_j R\right] \tag{11}$$

where λ is Lame's constant, μ is the shear modulus, ν is Poisson's ratio, δ_{ij} is the Kronecker delta, $R = \|\mathbf{x}-\mathbf{x}'\|$ is the Euclidean distance function, and $\partial_p = \partial/\partial x_p$. Substituting eqns. (10) and (11) into (9) gives

$$\sigma_{ij}^{I}(\mathbf{x}) = \frac{\mu b_m^I}{8\pi}\int_{L^I} \partial_n\partial_p\partial_p R\left(\epsilon_{nmi}\xi_j + \epsilon_{nmj}\xi_i\right)dl(\mathbf{x}') + \frac{\mu b_m^I}{4(1-\nu)}\int_{L^I} \xi_k\epsilon_{nmk}\left(\partial_n\partial_i\partial_j - \delta_{ij}\partial_n\partial_p\partial_p\right)Rdl(\mathbf{x}') \tag{12}$$

Eqn. (12) gives the stress field due to a discrete dislocation loop. For multiple dislocations $I = 1, 2, \ldots$, etc. distributing in the general 3D space, by the principle of elastic superposition, we have their total stress field given as

$$\sigma_{ij}(\mathbf{x}) = \sum_I \sigma_{ij}^I(\mathbf{x}) = \sum_I \begin{bmatrix} \frac{\mu b_m^I}{8\pi} \int_{L^I} \partial_n \partial_p \partial_p R\left(\epsilon_{nmi}\xi_j + \epsilon_{nmj}\xi_i\right) dl(\mathbf{x}') \\ + \frac{\mu b_m^I}{4(1-\nu)} \int_{L^I} \xi_k \epsilon_{nmk}\left(\partial_n \partial_i \partial_j - \delta_{ij}\partial_n \partial_p \partial_p\right) R dl(\mathbf{x}') \end{bmatrix} \tag{13}$$

In the "intensive" description of a dislocation microstructure, dislocation contents are represented by the dislocation density function $\boldsymbol{\rho}(\mathbf{x}')$ defined in eqn. (5). Thus, by the principle of elastic superposition, the stress field due to the dislocation content represented by $\boldsymbol{\rho}(\mathbf{x}')$ is obtainable from eqn. (13) by the substitution: $\sum_I b_i^I \xi_j^I(\mathbf{x}') dl = \alpha_{ij}(\mathbf{x}') dA dl = \alpha_{ij}(\mathbf{x}') dV$, where $\boldsymbol{\alpha}$ is the Nye tensor (Nye, 1953) $\alpha_{ij} = \sum_I b_i^I \xi_j^I / dA$, dA is defined in Fig. 2, and $dV = dA\, dl$ is an infinitesimal volume. The stress field is therefore:

$$\sigma_{ij}(\mathbf{x}) = \frac{\mu}{8\pi} \iiint \partial_n \partial_p \partial_p R\left(\alpha_{mj}\epsilon_{nmi} + \alpha_{mi}\epsilon_{nmj}\right) dV(\mathbf{x}') +$$

$$\frac{\mu}{4(1-\nu)} \iiint \alpha_{mk}\epsilon_{nmk}\left(\partial_n \partial_i \partial_j - \delta_{ij}\partial_n \partial_p \partial_p\right) R dV(\mathbf{x}') \tag{14}$$

2.2.2 Removing singularity in Mura's formula for "intensive" dislocation representation

Mura's formula breaks down when describing the elastic interaction between neighboring points, as some components of the stress field diverge as $R \to 0$. However, in the "intensive" dislocation description here, as mentioned in the Introduction, the pixel resolution should still be larger than the atomic size a. Thus, the $R \to 0$ condition is not allowed in the "intensive" picture and to ensure this, we adopt a strategy proposed by Cai and co-workers, albeit for DDD (Cai et al., 2006; Jamond et al., 2016; Po et al.,

2017), in which the R in eqn. (14) is replaced by another quantity R_a so that as $R \to 0$, $R_a \to a$ where a is a small length of atomic dimension. Formally, the following mapping is used between R and R_a (Cai et al., 2006):

$$R_a(\mathbf{x}) = \sqrt{R(\mathbf{x})^2 + a^2} \tag{15}$$

With R replaced by R_a, eqn. (14) becomes

$$\sigma_{ij}(\mathbf{x}) = \iiint K_{ij}^{3\mathrm{D}}(\mathbf{x}, \mathbf{x}', \boldsymbol{\alpha}(\mathbf{x}'))\, dV(\mathbf{x}') \tag{16}$$

with

$$K_{ij}^{3\mathrm{D}}(\mathbf{x}, \mathbf{x}', \boldsymbol{\alpha}(\mathbf{x}')) = \frac{\mu}{8\pi}\left(\alpha_{mj}\epsilon_{nmi} + \alpha_{mi}\epsilon_{nmj}\right)\partial_n\partial_p\partial_p R_a + \frac{\mu}{4(1-\nu)}\alpha_{mk}\epsilon_{nmk}\left(\partial_n\partial_i\partial_j - \delta_{ij}\partial_n\partial_p\partial_p\right)R_a$$

where

$$\partial_n\partial_p\partial_p R_a = -\frac{2(x_n - x_n')}{{R_a}^3}\left(1 + \frac{3a^2}{2{R_a}^2}\right)$$

and

$$\partial_n\partial_i\partial_j R_a = -\frac{\delta_{ij}(x_n - x_n') + \delta_{in}\left(x_j - x_j'\right) + \delta_{jn}(x_i - x_i')}{{R_a}^3} + \frac{3(x_n - x_n')\left(x_j - x_j'\right)(x_i - x_i')}{{R_a}^5} \tag{17}$$

2.2.3 Elastic interaction between dislocation densities on single slip plane

For the specific case where all the dislocation contents have the same Burgers vector **b** and reside on a given slip plane S of thickness b, the stress field in eqn. (14) can be reduced to

$$\sigma_{ij}(\mathbf{x}) = \iint_S K_{ij}(\mathbf{x}, \mathbf{x}', \boldsymbol{\rho}(\mathbf{x}'))\, dS(\mathbf{x}') \tag{18}$$

where

$$K_{ij}(\mathbf{x},\mathbf{x}',\boldsymbol{\rho}(\mathbf{x}')) = \frac{\mu b b_m}{8\pi}\left(\epsilon_{nmi}\rho_j + \epsilon_{nmj}\rho_i\right)\partial_n\partial_p\partial_p R_a + \frac{\mu b b_m}{4(1-\nu)}\rho_k\epsilon_{nmk}\left(\partial_n\partial_i\partial_j - \delta_{ij}\partial_n\partial_p\partial_p\right)R_a$$

b is the slip plane thickness and the $\partial_n\partial_i\partial_j R_a$ terms are still those given in eqn. (17). Eqn. (18) will be useful in the following discussion on dislocation core interactions.

2.2.4 Glide stress τ^{dis} for dislocation dynamics

Next, we proceed to work out the glide stress $\tau^{\mathrm{dis}}(\mathbf{x})$ in eqn. (8) due to mutual-dislocation interactions. Since the glide stress in eqn. (8) is used for the dislocation velocity in eqn. (7), in the following, the field point **x** is understood to be a location where some dislocation contents would reside. In the "intensive" picture, **x** would then be a point inside the core of a unit dislocation, and τ^{dis} would then be made up of a component τ^{unit} due to elastic interactions from all other unit-dislocation contents outside the core of the dislocation where **x** is situated, and a component τ^{core} due to interactions (both elastic and misfit; see later) with dislocation contents inside the dislocation core where **x** resides, i.e.

$$\tau^{\mathrm{dis}}(\mathbf{x}) = \tau^{\mathrm{unit}}(\mathbf{x}) + \tau^{\mathrm{core}}(\mathbf{x}) \tag{19}$$

2.2.4.1 Glide stress τ^{unit} due to elastic interactions from outside core

τ^{unit} is given as the resolved shear stress of the stress tensor σ_{ij} due to elastic interactions with all other unit-dislocation contents, i.e.

$$\tau^{\mathrm{unit}}(\mathbf{x}) = n_i\sigma_{ij}(\mathbf{x})b_j \tag{20}$$

where $\{b_j, n_i\}$ specifies the slip system under consideration, and the stress tensor σ_{ij} is given by either eqn. (16) if the interacting dislocation contents reside on a 3D space (i.e. multiple slip), or eqn. (18) if they are on the same (2D) slip plane as the dislocation density at the field point **x**. Thus, writing out formally, the σ_{ij} in eqn. (20) is:

$$\sigma_{ij}(\mathbf{x}) = \iiint_{V-\text{core}} K_{ij}^{\text{3D}}(\mathbf{x}, \mathbf{x}', \boldsymbol{\alpha}(\mathbf{x}'))\, dV(\mathbf{x}') \quad \text{or} \quad \iint_{S-\text{core}} K_{ij}(\mathbf{x}, \mathbf{x}', \boldsymbol{\rho}(\mathbf{x}'))\, dS(\mathbf{x}') \tag{21}$$

where integration is over domain (3D or 2D) excluding the dislocation core, in which the interactions will be considered separately. The K_{ij}^{3D} or K_{ij} here is that given by eqns. (16) and (18) respectively.

2.2.4.2 Glide stress τ^{core} due to interactions inside core

As mentioned in Section 1, the "intensive" representation of dislocations serves to model the interactions within the dislocation core, for which "extensive" and "discrete" representations fail to provide a description (Leung and Ngan, 2016). Within the dislocation core the dislocation contents are subjected to not only their mutual elastic interaction, but also a lattice mismatch force arising from interaction with the crystal lattice (Peierls, 1940), so that τ^{core} may be written as:

$$\tau^{\text{core}}(\mathbf{x}) = n_i b_j \iint_{\text{core}} K_{ij}(\mathbf{x}, \mathbf{x}', \boldsymbol{\rho}(\mathbf{x}'))\, dS(\mathbf{x}') + \tau^{\text{misfit}}(\mathbf{x}) \tag{22}$$

where the first term is due to elastic interaction within the core, with $K_{ij}(\mathbf{x}, \mathbf{x}', \boldsymbol{\alpha}(\mathbf{x}'))$ given by eqn. (18), and τ^{misfit} is the glide stress due to lattice misfit. Within the concept of the generalized stacking-fault-energy surface $\gamma(\mathbf{u})$ (Christian and Vítek, 1970; Vítek and Kroupa, 1969), the restoring shear stress due to a disregistry displacement **u** on the slip plane is $-\boldsymbol{\nabla}_{\mathbf{u}}\gamma$, and this will produce a glide stress of

$$\tau^{\text{misfit}}(\mathbf{x}) = -\hat{\mathbf{b}} \cdot \boldsymbol{\nabla}_{\mathbf{u}}\gamma|_{\mathbf{u}(\mathbf{x})} \tag{23}$$

on the slip system $\{\mathbf{b}, \hat{\mathbf{n}}\}$. For general curved dislocations, evaluation of τ^{misfit} using eqn. (23) would require first solving the plastic displacement vector field $\mathbf{u}(\mathbf{x})$ from the Nye tensor $\boldsymbol{\alpha}(\mathbf{x})$ via the following equation (see Appendix A):

$$\boldsymbol{\nabla} \times [\boldsymbol{\nabla} \otimes \mathbf{u}(\mathbf{x})] = -\boldsymbol{\alpha}(\mathbf{x}) \tag{24}$$

where $\otimes$ is the tensor product operator. Unfortunately, solution of eqn. (24) from known boundary conditions is too computationally expensive (Gbemou et al., 2016; Roy and Acharya, 2005).

Thus, instead of starting from the $\gamma(\mathbf{u})$ surface and working out τ^{misfit} from eqn. (23), we devise a more efficient method here. Recall that within the dislocation core, the misfit interaction counterbalances the elastic interaction to result in a stable shape of the core. Thus, in eqn. (22), τ^{misfit} is proposed to take the form:

$$\tau^{\text{misfit}}(\mathbf{x}) = -n_i b_j \iint_{\text{core}} K_{ij}(\mathbf{x}, \mathbf{x}', \boldsymbol{\rho}(\mathbf{x}'))\, f(d(\mathbf{x}, \mathbf{x}'))\, dS(\mathbf{x}') \tag{25}$$

where $d(\mathbf{x}, \mathbf{x}') = \left\| (\mathbf{x} - \mathbf{x}') \cdot \left(\hat{\mathbf{n}} \times \hat{\boldsymbol{\xi}} \right) \right\|$ is the spacing between the field point $\mathbf{x}$ and source point $\mathbf{x}'$ projected along the width direction $\hat{\mathbf{n}} \times \hat{\boldsymbol{\xi}}$ of the dislocation core. Compare with the first term in eqn. (22), the τ^{misfit} in eqn. (25) is essentially the elastic interaction scaled by a factor $f(d)$, and eqn. (22) now reads:

$$\tau^{\text{core}}(\mathbf{x}) = n_i b_j \iint_{\text{core}} K_{ij}(\mathbf{x}, \mathbf{x}', \boldsymbol{\rho}(\mathbf{x}'))\, [1 - f(d(\mathbf{x}, \mathbf{x}'))]\, dS(\mathbf{x}') \tag{26}$$

The factor $f(d)$ in eqn. (26) serves two important roles: (i) it stabilizes the core into a given shape, and (ii) by doing so in a dynamic fashion, it also gives rise to a minimum applied stress required to move the dislocation, i.e. a stress that mimics the so-called lattice friction or Peierls stress.

Let $h(\hat{\boldsymbol{\xi}})$ be the steady-state half core width corresponding to a given dislocation character $\hat{\boldsymbol{\xi}}$, to play a stabilizer role $f(d)$ may have the following characteristics:

$$f(d)\begin{cases} > 1 & \text{if } d > h(\hat{\boldsymbol{\xi}}) \\ < 1 & \text{if } d < h(\hat{\boldsymbol{\xi}}) \\ = 1 & \text{if } d = h(\hat{\boldsymbol{\xi}}) \end{cases} \tag{27}$$

so that if the source and field points are separated farther than half the core width, then a net attractive force ($f > 1$) exists to pull the densities back together, but if they are too close together, a net repulsive force ($f < 1$) acts to push the densities apart, and the self interaction at a given point is according to K_{ij}, which is already non-singular due to eqn. (15), without additional opposing force ($f = 1$). The core shape dictated by such a form of $f(d)$ would then have a stable width but tend to dissociate into partials – a possible form for $f(d)$ which would result in these will be suggested later in Section 4. It may be criticized that this method of modeling the core shape is less rigorous than the γ-surface approach mentioned above, but it must also be remembered that the $\gamma(\mathbf{u})$ surface is itself a concept that is only approximately valid. In particular, previous criticisms of the γ-surface concept include the ignorance of the effects of the high gradients in $\mathbf{u}(\mathbf{x})$ in the dislocation core (Bullough and Tewary, 1979) and, more importantly, the fact that the $\gamma(\mathbf{u})$ surface cannot be unambiguously defined or computed with high accuracy, due to the constraints needed to maintain the crystal configuration at a general disregistry $\mathbf{u}$ that does not correspond to a ground state (Ngan, 1995). In fact, the form of the interaction in eqn. (25) is not mathematically inconsistent with the γ-surface concept, because $f(d)$ in eqn. (25) may be regarded as a function that best fits eqn. (25) to eqn. (23). For example, $f(d)$ may be represented as a power series in d:

$$f(d) = \sum_n a_n \left[d/h(\hat{\boldsymbol{\xi}})\right]^n \tag{28}$$

with $\sum_n a_n = 1$ which guarantees $f\left(d = h(\hat{\boldsymbol{\xi}})\right) = 1$. The coefficients a_n may then be chosen to result in a suitable structure of the dislocation core in a given material.

2.3 Summary

To summarize, the following equations close the problem of the dynamics of "intensive" dislocations gliding on their slip planes:

(i) Dynamics equation for dislocation density:

$$\dot{\boldsymbol{\rho}} = \dot{\rho}_e \hat{\mathbf{x}}_e + \dot{\rho}_s \hat{\mathbf{x}}_s = -\frac{\partial(\rho v)}{\partial \mathbf{x}_e}\hat{\mathbf{x}}_s + \frac{\partial(\rho v)}{\partial \mathbf{x}_s}\hat{\mathbf{x}}_e \tag{6}$$

(ii) Dislocation velocity:

$$v = \mathrm{sgn}\left(\tau^{\mathrm{eff}}\right) v_0 \left|\tau^{\mathrm{eff}}/\tau_0\right|^m \tag{7}$$

(iii) Effective glide stress:

$$\tau^{\mathrm{eff}}(\mathbf{x}) = \tau^{\mathrm{ext}}(\mathbf{x}) + \tau^{\mathrm{unit}}(\mathbf{x}) + \tau^{\mathrm{core}}(\mathbf{x}) \tag{8, 19}$$

(iv) Glide stress due to elastic interactions from outside core:

$$\tau^{\mathrm{unit}}(\mathbf{x}) = n_i b_j \iiint_{V-\mathrm{core}} K_{ij}^{3D}(\mathbf{x}, \mathbf{x}', \boldsymbol{\alpha}(\mathbf{x}'))\, dV(\mathbf{x}') \quad \text{or} \quad n_i b_j \iint_{S-\mathrm{core}} K_{ij}(\mathbf{x}, \mathbf{x}', \boldsymbol{\rho}(\mathbf{x}'))\, dS(\mathbf{x}'), \tag{20, 21}$$

depending on whether the problem is 3D or 2D for a single slip plane, respectively. Here,

$$K_{ij}^{3D}(\mathbf{x}, \mathbf{x}', \boldsymbol{\alpha}(\mathbf{x}')) = \frac{\mu}{8\pi}\left(\alpha_{mj}\epsilon_{nmi} + \alpha_{mi}\epsilon_{nmj}\right)\partial_n\partial_p\partial_p R_a + \frac{\mu}{4(1-\nu)}\alpha_{mk}\epsilon_{nmk}\left(\partial_n\partial_i\partial_j - \delta_{ij}\partial_n\partial_p\partial_p\right)R_a$$

$$K_{ij}(\mathbf{x}, \mathbf{x}', \boldsymbol{\rho}(\mathbf{x}')) = \frac{\mu b b_m}{8\pi}\left(\epsilon_{nmi}\rho_j + \epsilon_{nmj}\rho_i\right)\partial_n\partial_p\partial_p R_a + \frac{\mu b b_m}{4(1-\nu)}\rho_k\epsilon_{nmk}\left(\partial_n\partial_i\partial_j - \delta_{ij}\partial_n\partial_p\partial_p\right)R_a$$

$$\partial_n\partial_p\partial_p R_a = -\frac{2(x_n - x_n')}{{R_a}^3}\left(1 + \frac{3a^2}{2{R_a}^2}\right),$$

$$\partial_n\partial_i\partial_j R_a = -\frac{\delta_{ij}(x_n - x_n') + \delta_{il}\left(x_j - x_j'\right) + \delta_{jl}(x_i - x_i')}{{R_a}^3} + \frac{3(x_n - x_n')\left(x_j - x_j'\right)(x_i - x_i')}{{R_a}^5} \tag{16, 17, 18}$$

(v) Glide stress due to interactions inside core:

$$\tau^{\text{core}}(\mathbf{x}) = n_i b_j \iint_{\text{core}} K_{ij}(\mathbf{x}, \mathbf{x}', \boldsymbol{\rho}(\mathbf{x}'))\,[1 - f(d(\mathbf{x}, \mathbf{x}'))]\, dS(\mathbf{x}') \tag{26}$$

where $f(d)$ is a function that meets the characteristics in eqn. (27) or similar.

3 Numerical implementation for single slip plane

Here, we employ the framework outlined in Section 2.3 above to simulate 2D cases where dislocation contents of the same Burgers vector **b** reside on a given slip plane. In such a case, the 2D version of eqn. (21) is used for the elastic interaction between dislocation contents outside dislocation cores:

$$\tau^{\text{unit}}(\mathbf{x}) = n_i b_j \iint_{S-\text{core}} K_{ij}(\mathbf{x}, \mathbf{x}', \boldsymbol{\rho}(\mathbf{x}'))\, dS(\mathbf{x}') \tag{29}$$

In addition, computation of stress vis eqn. (29) can be further simplified by decoupling **ρ** into two components $\boldsymbol{\rho}_e$ and $\boldsymbol{\rho}_s$ as per eqn. (5), since edge and screw contents do not interact (Leung et al., 2015). In eqn. (26), the following $f(d)$ function that satisfies eqn. (27) is employed:

$$f(d) = (d/h)^n \tag{30}$$

where h is set to be dependent of dislocation character, and $n = 2$ unless otherwise stated. Eqn. (30) is in fact a special case of the power series in eqn. (28). Further details in methodology are explained below.

3.1 Method to determine inner or outer core interaction

Referring to eqn. (19) in Section 2.3, for a general field point **x** and a source point $\mathbf{x}'$ on the slip plane, a method needs to be devised to distinguish whether they belong to the same dislocation core or not, for which τ^{core} or τ^{unit} would apply respectively. Dislocation densities in the same core should have

the same direction, i.e. $\boldsymbol{\rho}(\mathbf{x}) \cdot \boldsymbol{\rho}(\mathbf{x}') > 0$ and is continuous with respect to space. Since the dislocation density vector is decomposed into edge and screw parts, the determination method here ought to be able to distinguish the core according to its edge and screw densities as well. For a given field point **x** with a non-zero dislocation density shown as the orange pixel in Fig. 3, if $|\rho_e/\rho_s| \leq 1$ there, we then decide whether $\boldsymbol{\rho}_s(\mathbf{x}')$ at pixels $\mathbf{x}'$ around a mid-axis (the red dash-dot axis) passing through **x** along the screw direction is in the same dislocation core as $\boldsymbol{\rho}_s(\mathbf{x})$. Moving out from the mid-axis in a perpendicular direction, if $\rho_s(\mathbf{x})\,\rho_s(\mathbf{x}') \leq 0$ is first satisfied we meet and mark the periphery of the dislocation core zone for the screw contents. Otherwise if $|\rho_e/\rho_s| \geq 1$ at point **x**, we begin with a mid-axis along $\boldsymbol{\rho}_e(\mathbf{x})$ and determine the periphery of the core zone for the edge contents. The dislocation densities in the same core zone are set to interact via τ^{core} in eqn. (26); otherwise they interact via τ^{unit} in eqn. (20, 21).

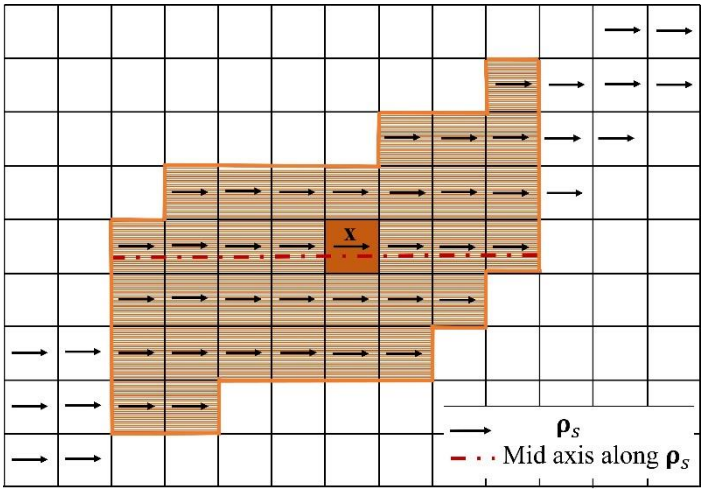

Fig. 3. Schematic for identifying dislocation core according to screw dislocation contents. The orange cell is the center point **x**, the red dash-dot line is the mid-axis which is parallel to the Burgers vector, and the orange contour shows the periphery of the dislocation core according to its screw contents.

3.2 Divergence-preserving finite volume method

It is important to choose a desirable numerical implement to solve divergence preserving equations because traditional finite-element or finite-volume methods, while conserving mass, introduce large divergence errors. Much efforts have been made in the past to solve divergence preserving equations numerically (Artebrant and Torrilhon, 2008; Torrilhon, 2005) and here, we adopt the potential-based approach finite volume method (Mishra and Tadmor, 2010) for solving eqn. (6). The two-dimensional form of the curl advection as in eqn. (6) can be written as

$$\begin{cases} \frac{d}{dt}\rho_x + f_y = 0 \\ \frac{d}{dt}\rho_y - f_x = 0 \end{cases} \tag{31}$$

where flux $\boldsymbol{f} = \boldsymbol{\rho} \times \mathbf{v}$ with f_x, f_y being its components in the x and y direction respectively. For the discretization, we adopt a uniform Cartesian mesh with sizes Δx and Δy. The discrete cell $C_{i,j} = \left[x_{i-\frac{1}{2}}, x_{i+\frac{1}{2}}\right) \times \left[y_{j-\frac{1}{2}}, y_{j+\frac{1}{2}}\right)$ centers at the mesh point $(x_i, y_i) = (i\Delta x, j\Delta y)$. A potential based semi-discrete finite-volume scheme for eqn. (31) is

$$\begin{cases} \frac{d}{dt}(\rho_x)_{i,j} = -\frac{1}{4\Delta y}\left(\mu_x F^x_{i,j+1} - \mu_x F^x_{i,j-1}\right) - \frac{1}{4\Delta y}\left[\delta_y\left(\mu_x F^y_{i+\frac{1}{2},j} + \mu_x F^y_{i-\frac{1}{2},j}\right)\right] \\ \frac{d}{dt}(\rho_y)_{i,j} = \frac{1}{4\Delta x}\left(\mu_y F^y_{i+1,j} - \mu_y F^y_{i-1,j}\right) + \frac{1}{4\Delta x}\left[\delta_x\left(\mu_y F^x_{i,j+\frac{1}{2}} + \mu_y F^x_{i,j-\frac{1}{2}}\right)\right] \end{cases} \tag{32}$$

Here, μ_x, μ_y, δ_x and δ_y are standard discrete averaging and difference operators in the finite-volume method given as

$$\begin{cases} \mu_x a_{I,J} \coloneqq \frac{a_{I+\frac{1}{2},J} + a_{I-\frac{1}{2},J}}{2}, & \mu_y a_{I,J} \coloneqq \frac{a_{I,J+\frac{1}{2}} + a_{I,J-\frac{1}{2}}}{2} \\ \delta_x a_{I,J} \coloneqq a_{I+\frac{1}{2},J} - a_{I-\frac{1}{2},J}, & \delta_y a_{I,J} \coloneqq a_{I,J+\frac{1}{2}} - a_{I,J-\frac{1}{2}} \end{cases} \tag{33}$$

where a represents an arbitrary variable and the indexes I and J are at the center $I=i$, $J=j$ or at the edge $I = i \pm \frac{1}{2}, J = j \pm \frac{1}{2}$. $F^x_{i+\frac{1}{2},j}$ and $F^y_{i,j+\frac{1}{2}}$ are edge centered numerical fluxes:

$$\begin{cases} F^{x}_{i+\frac{1}{2},j} = \mu_x f_{i+\frac{1}{2},j} + Q^{x}_{i+\frac{1}{2},j}\delta_x(\rho_y)_{i+\frac{1}{2},j} \\ F^{y}_{i,j+\frac{1}{2}} = \mu_y f_{i,j+\frac{1}{2}} - Q^{y}_{i,j+\frac{1}{2}}\delta_y(\rho_x)_{i,j+\frac{1}{2}} \end{cases} \tag{34}$$

We adopt the first-order Rusanov flux for Q^x and Q^y in eqn. (34):

$$\begin{cases} Q^{x}_{i+\frac{1}{2},j} = \max\{|\lambda^{y}_{i,j}|, |\lambda^{y}_{i+1,j}|\} \\ Q^{y}_{i,j+\frac{1}{2}} = \max\{|\lambda^{x}_{i,j}|, |\lambda^{x}_{i,j+1}|\} \\ |\lambda^{l}_{i,j}| = \left|\frac{\partial f}{\partial \rho_l}\right| \end{cases} \tag{35}$$

The time integration is performed by the Runge–Kutta method and the following time step is chosen to ensure convergence of the simulation

$$d_t = \frac{d_x}{1.25\max\left(\max(|v_x|),\max(|v_y|)\right)} \tag{36}$$

3.3 Simulation details

We used the MATLAB language to develop the model and the parameters, which correspond to aluminum, are shown in Tables 1 and 2.

Table 1. Parameters in the simulation

Parameters	values
Shear modulus μ	26 GPa
Poisson's ratio ν	0.3
Burgers vector b	2.863×10^{-10} m
m for dislocation velocity	1
v_0 for dislocation velocity	v^*
τ_0 for dislocation velocity	$1.9231\times10^{-4}\ \mu$
Slip plane dimensions (with periodic boundary condition)	300 b×300 b
Number of cells (n_x×n_y)	300×300
Unit cell dimension (d_x×d_y)	1 b×1 b

Cut-off radius for elastic interaction	300 b
a for non-singularity improvement	1.25 d_x (1.25 b)
Equilibrium half-width of the dislocation h	$3d_x$ for edge dislocation $3(1-\nu)d_x$ for screw dislocation
Unit dislocation density ρ_s	$1/d_x$ ($1/b$)
Truncation value of dislocation density	$\rho_s \times 10^{-6} \sim \rho_s \times 10^{-4}$

Table 2. Characteristic scales for normalization of parameters

Quantities	Characteristic scales for normalization
Length l^*	b
Time t^*	1×10^{-9} s
Velocity v^*	$v^*=l^*/t^*$
Stress τ^*	$\tau^*=\mu$

4. Simulation results

4.1 Equilibrium density distribution of dislocation cores and Peierls stress

4.1.1 Equilibrium core shape and γ-surface

To demonstrate the validity of our core interaction method, we obtain the equilibrium distributions of straight dislocation cores without external stress. Such states were produced by running the simulation according to the dynamic scheme in Section 2.3 albeit for straight dislocations under no external stress, until dynamic equilibrium was observed for the shape of the dislocation core. Instead of using eqn. (22, 23) and the condition $\rho_i = \partial u_i/\partial x_i$ to solve the equilibrium distribution for straight dislocations, we employed the following equations from the classical Peierls model (Peierls, 1940) which are valid for straight dislocations. At equilibrium under zero external stress, the γ-surface is related to the equilibrium density distribution by

$$A\int_{-\infty}^{+\infty}\frac{\rho(x')}{x-x'}dx' = -\frac{d\gamma}{du} \tag{37}$$

where $A = \mu b/[2\pi(1-\nu)]$ for edge or $\mu b/(2\pi)$ for screw character, respectively, x is the coordinate along the width direction of the dislocation, and u is the disregistry along the edge or screw direction given by

$$u(x) = \int_{-\infty}^{x} \rho(x')dx' \tag{38}$$

From eqns. (37) and (38), given the equilibrium density distribution $\rho(x)$ from the simulation, we can obtain the corresponding disregistry function $u(x)$ and the γ-surface $\gamma(u)$ numerically.

To see how the $f(d)$ function affects the equilibrium distribution of dislocation density inside the core, we employ eqn. (30) for $f(d)$ and examine how n and h influence the equilibrium shape of the dislocation core. Fig. (4) shows the core structure at different values of n for edge dislocations, when $h = 10\ b$. It can be seen that the n value determines the sharpness of the two dissociated partials: the $n = 2$ case exhibits two overlapping partials, while the $n = 15$ case exhibits clear dissociation of the unit dislocation into two narrow partials. Fig. (5) shows the core distribution of edge dislocations of different equilibrium half width h and suitable n value that would allow more distinctive dissociation, as well as the corresponding sections of the γ-surface calculated via eqns. (37) and (38). The results shows that a larger h in $f(d)$ corresponds to a large width in the dislocation core and the local minimum in the γ-surface, and yet the peak energy in the γ-surface is also lowered.

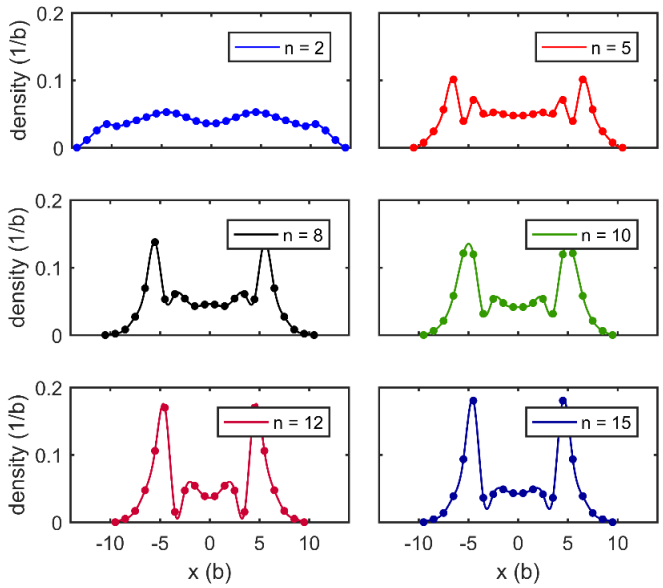

Fig 4. Dislocation density distributions for edge dislocations at different *n*.

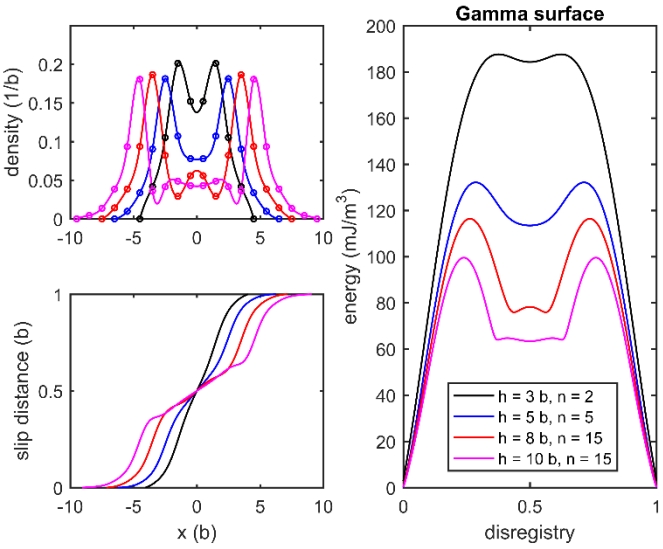

Fig 5. Dislocation density and disregistry (slip distance) distributions, and γ-surfaces for edge dislocations at different equilibrium half width *h*.

In order to investigate dislocations in aluminum, parameters $a = 1.25\,b$, $n = 2$ and $h = 3\,b$ were adopted for edge dislocation and $a = 1.25\,b$, $n = 2$ and $h = 3(1-\nu)\,b$ for screw dislocation via the equations in Section 2.3. As shown in Fig. 6, the edge dislocation core has a wider distribution and tends to dissociate into two partials (Woodward et al., 2008) while no apparent dissociation occurs in the screw dislocation core (Lu et al., 2000). The spacing between the two partials in the edge dislocation is around 3b (8.05 Å) which is close to the experimental value of 8 Å (Höllerbauer and Karnthaler, 1981) and density-functional theory (DFT) prediction of 7.0-9.5 Å (Woodward et al., 2008) or 20.4 Å (Shin and Carter, 2013). For the screw dislocation core with no obvious dissociation, the half width, which is defined as the distance where the atomic disregistry changes from 1/4 *b* to 3/4 *b* (Lu et al., 2000), is predicted to be 2.4 *b* (6.8712 Å), which is reasonable in comparison with the literature value of 2.1 Å (Lu et al., 2000) (no dissociation predicted) and 5-7.5 Å (Woodward et al., 2008) (dissociation predicted) from DFT studies. The γ-surface plots in Fig. 6 exhibit maximum energy of 187 mJ/m^3 in the [1 1 $\bar{2}$] direction and 172 mJ/m^3 in the [1 $\bar{1}$ 0] direction. Two minor peaks are observed in the [1 1 $\bar{2}$] direction and they are responsible for the splitting of the edge dislocation into two partials.

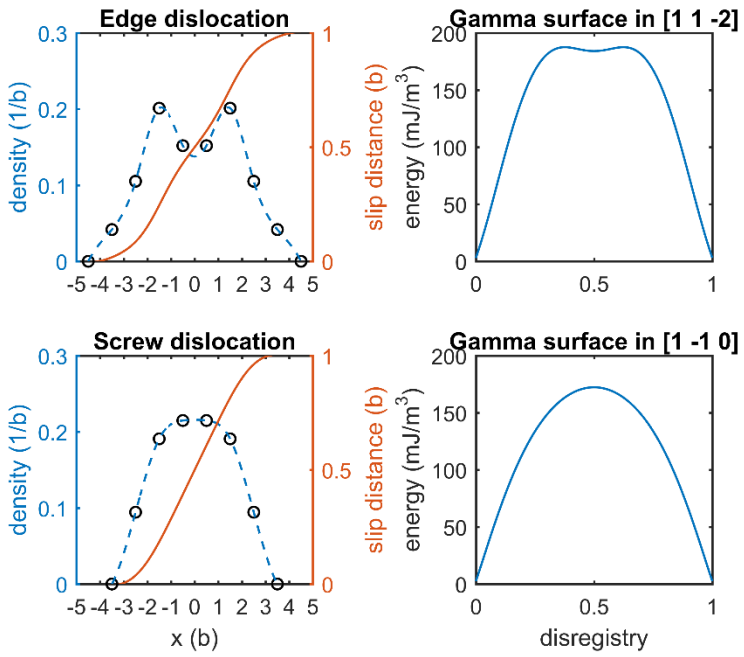

Fig 6. Dislocation density and disregistry (slip distance) distributions, and γ-surfaces for edge and screw straight dislocations.

4.1.2 Stress distribution within dislocation core

The stress field in the present model may also be compared with other dislocation models. Here, we take the edge dislocation and consider the stress field on the slip plane as an example. In the singular Volterra model, the density distribution of an edge dislocation is a delta function, and the stress field on the slip plane $y = 0$ is

$$\sigma_{xy}(x, y = 0) = \frac{\mu b}{2\pi(1-\nu)}\frac{1}{x} \tag{39}$$

In the Peierls-Nabarro (P-N) model, the stress field for an edge dislocation with half width h is

$$\sigma_{xy}(x, y = 0) = \frac{\mu b}{2\pi(1-\nu)}\frac{x}{x^2+h^2} \tag{40}$$

In the present model, by virtue of Cai's non-singular improvement in eqn. (15), the elastic stress field outside the core is given by

$$\sigma_{xy}(x, y = 0) = \frac{\mu b}{2\pi(1-\nu)} \frac{x}{x^2+a^2} \tag{41}$$

while that inside the core is

$$\sigma_{xy}(x, y = 0) = \int_{-h}^{+h} \rho(x') \frac{\mu b(x-x')}{2\pi(1-\nu)[(x-x')^2+a^2]} dx' \tag{42}$$

Fig. 7 shows the elastic stress calculated according to eqn. (42) for one dynamic equilibrium state simulated with $a = 1.25\, b$, $n = 2$ and $h = 3\, b$, in comparison with the Volterra model from eqn. (39) and the P-N model from eqn. (40). It can be seen that the stress field predicted by the present model does not exhibit a singularity in the dislocation core as in the Volterra model, and since the core width is more well-defined than the P-N model, the stress field agrees more with the Volterra model outside the core region. However, it must also be noted that in the present model, the core distribution is adjustable by the simulation parameters as in Figs. 4-6, and hence other stress profiles are possible. Also shown in Fig. 7 is the *total* stress in the core region which is given as

$$\sigma_{xy}^{\text{total}}(x, y = 0) = \int_{-h}^{+h} \rho(x') \frac{\mu b(x-x')}{2\pi(1-\nu)[(x-x')^2+a^2]} (1 - f(d(x, x')))dx' \tag{43}$$

where the $f(d)$ term represents the lattice misfit interaction. It can be seen that although the net stress is very small everywhere within the core, indicating that the core is approximately at equilibrium.

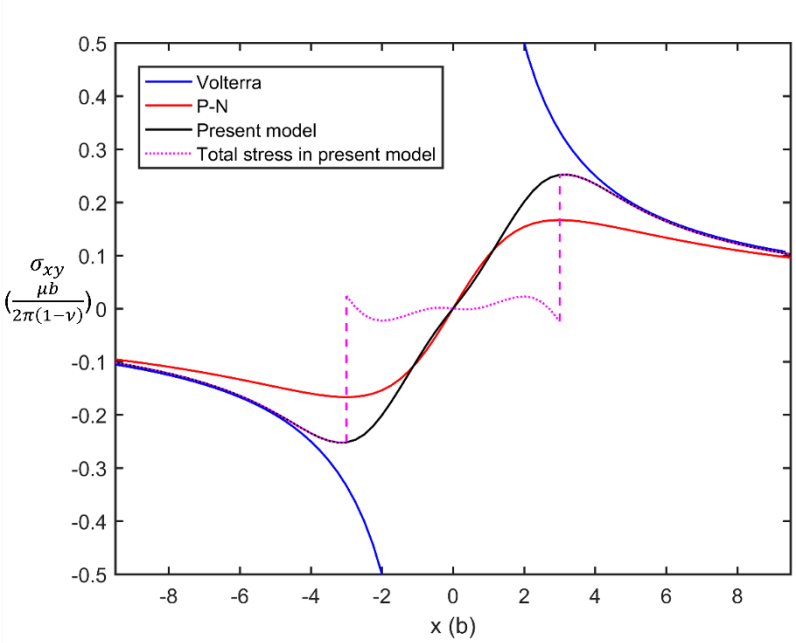

Fig. 7. Comparison of elastic stress on slip plane between the present model, the Volterra model, and the Peierls-Nabarro (P-N) model for an edge dislocation with dislocation half width $h = 3\,b$, $a = 1.25\,b$ and $n = 2$. The jumps in the total stress show the boundaries of the dislocation core.

4.1.3 Peierls stress

As mentioned above, an important difference between the "discrete" and "intensive" descriptions of dislocations is that the "discrete" picture fails to give intrinsic information about the Peierls stress, while in the "intensive" picture, since the core of the dislocation is modeled, so can be the Peierls stress. In the classical P-N model, as the dislocation traverses both the strain energy and the misfit energy would remain constant if they are calculated by continuous integration over the slip plane (Hirth and Lothe, 1982), and hence no Peierls stress would be predicted. This is because in the P-N model, there is no provision for the core to change shape as it traverses. Peierl and Nabarro managed to obtain a non-zero lattice friction only by replacing the continuous integration by discrete summation over lattice sites in the calculation of the

misfit energy, but this approach was challenged (Hirth and Lothe, 1982.). Indeed, in continuum models, the Peierls-Nabarro way of discrete summation would be an incompatible approach, and unless the dislocation core is made to change shape as it traverses, no Peierls stress could be predicted.

As mentioned in Section 2.2.4.2, the $f(d)$ factor in eqn. (26) serves not only to preserve the width of the dislocation, but also to cause a critical stress that mimics the Peierls stress to move the dislocation. Fig. 8 shows that, because of the width-stabilizing role of the $f(d)$ factor, as a stress of increasing magnitude is applied onto the crystal, the dislocation core first changes its shape but without moving, and only when a critical stress is applied then the dislocation starts to move. In the set of results in Fig. 6, the Peierls stress was obtained by finding the lower and upper bounds of the critical shear stress needed to move the dislocation. The interval is found for edge and screw dislocations to be 1.75×10^{-3}-2.2×10^{-3} μ, lying in the range of 10^{-5}-10^{-2} μ (Shin and Carter, 2013) reported from simulations, larger than the 10^{-5}-10^{-4} μ (Seeger et al., 1966) from mechanical tests, and agreeing with 10^{-3}-10^{-2} μ (Benoit et al., 1987; Nabarro, 1997) from typical Bordoni peaks in internal friction measurements.

In eqn. (30), the value of $f(d) = [d/h]^n$ increases as n increases or h decreases. The $f(d)$ factor not only decides the configuration of the core, but also influences the Peierls stress. Fig. 9 shows the Peierls stress simulated for edge dislocations with different n and h, and it can be seen that the Peierls stress increases as n increases or h decreases. The reduction of the Peierls stress as h decreases is in good agreement with conventional physical understanding – as the dislocation width increases, the strain of the dislocation is more spread out and hence fluctuations in core shape and energy would be less as a stress is applied or as the dislocation moves. Fig. 9 shows that, with suitable choice of the parameters n and h, a desired lattice friction can be simulated in the present scheme, and this has not been made possible before in any purely continuum framework for dislocation dynamics.

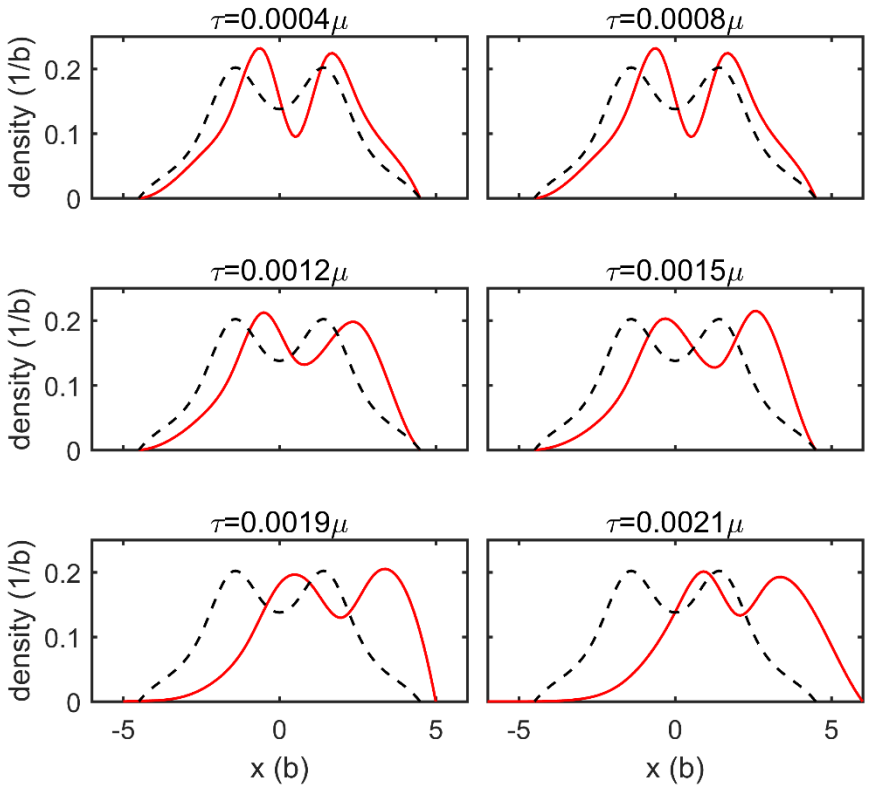

Fig. 8. Equilibrium dislocation density profiles for edge dislocation at different external resolved shear stress τ before reaching the critical Peierls stress (red curves). The dislocation half width $h = 3\ b$, $a = 1.25\ b$ and $n = 2$. The black dashed curves show the density distribution at zero external stress for comparison.

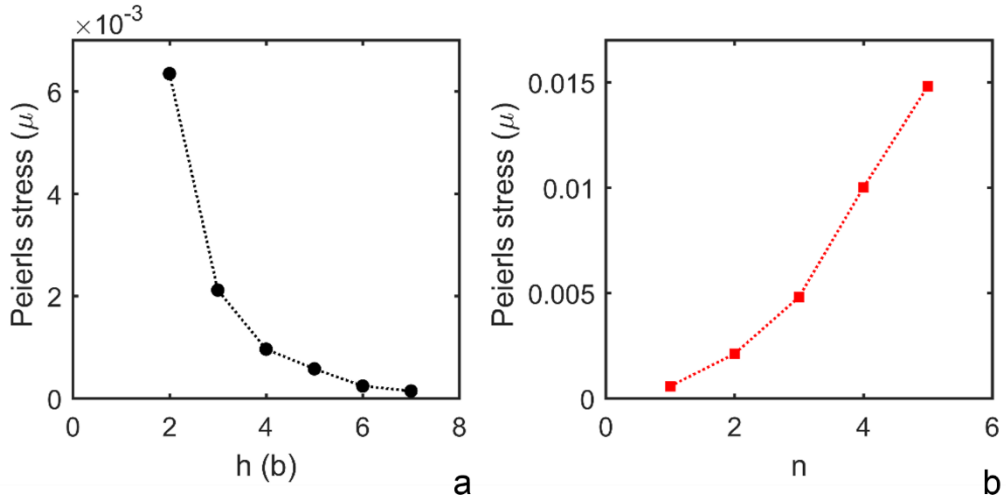

Fig. 9. Simulated Peierls stress for edge dislocation, (a) with different dislocation half width h at $n = 2$, and (b) different n values at $h = 3$ b.

4.2 Simulation of dislocation mechanisms

Next, we study how well the present modeling framework applies to expansion and shrinkage of loops, Frank-Read source and Orowan looping.

4.2.1 Loop expansion and shrinkage

Testing the new model by loop shrinkage and expansion is crucial as this will reveal whether the self stress, which drives shrinkage and opposes expansion, and the continuity of the dislocation density are properly depicted. Fig. 10(a) shows the simulated shrinkage of a dislocation loop under the sole influence of its self stress without externally applied stress, and Fig. 10(b) shows the expansion of the same loop under an applied shear stress. The initial loop for both cases is the same, and beginning from such a state, in both the shrinkage and expansion cases, the loop evolves into an elliptical shape because with the Poisson ratio ν of 0.3 used in the simulations, the interaction between the screw character

(horizontal in Fig. 10) is larger than that between the edge character (vertical in Fig. 10). In either cases, it can be seen that the continuity of the dislocation density along the loop is well maintained, and the fact that the loop shrinks smoothly indicates that the self stress is depicted satisfactorily.

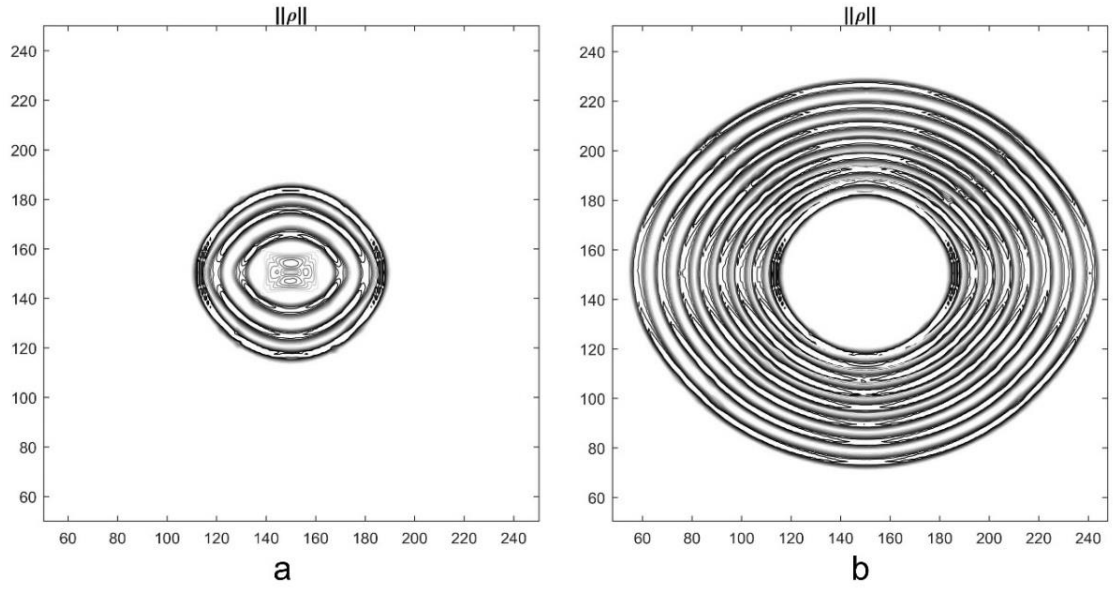

Fig. 10. (a) Shrinkage of a single loop under self stress, and (b) expansion of a loop under an applied shear stress 0.0308 μ. The initial loop for both situations is the same which is the largest one in the shrinkage case and the smallest one in the expansion case. Screw direction is horizontal in both cases.

4.2.2 Frank-Read source

In the second example of simulating a Frank-Read source, in addition to self stress and continuity, whether annihilation can be correctly modeled can also be tested. In the simulation, as shown in Fig. 11, the Frank-Read source is initially a short screw dislocation segment pinned at both ends on the slip plane, and the periodic boundary conditions are applied in two dimensions. As can be seen from Fig. 11, the initial screw segment bows out on the slip plane as a shear stress is applied. In the initial condition, the

divergence of every point on the continuous dislocation line is zero, except at two end-points where the divergence is non-zero. As the simulation runs, the special FVM employed preserves the divergence as in the initial condition, so that as the dislocation bows out, the two pins stay without having to apply extra stress or reset the velocity there. On increasing applied stress, the dislocation expands and loops around, and then annihilation takes place when the segments with opposite signs meet each other, in exactly the way as a Frank-Read source would do.

Simulations of loop shrinkage/expansion and Frank-Read source operation were also performed using a Discrete Dislocation Dynamics solver, and comparison of the results with the present modeling framework is made in Appendix B.

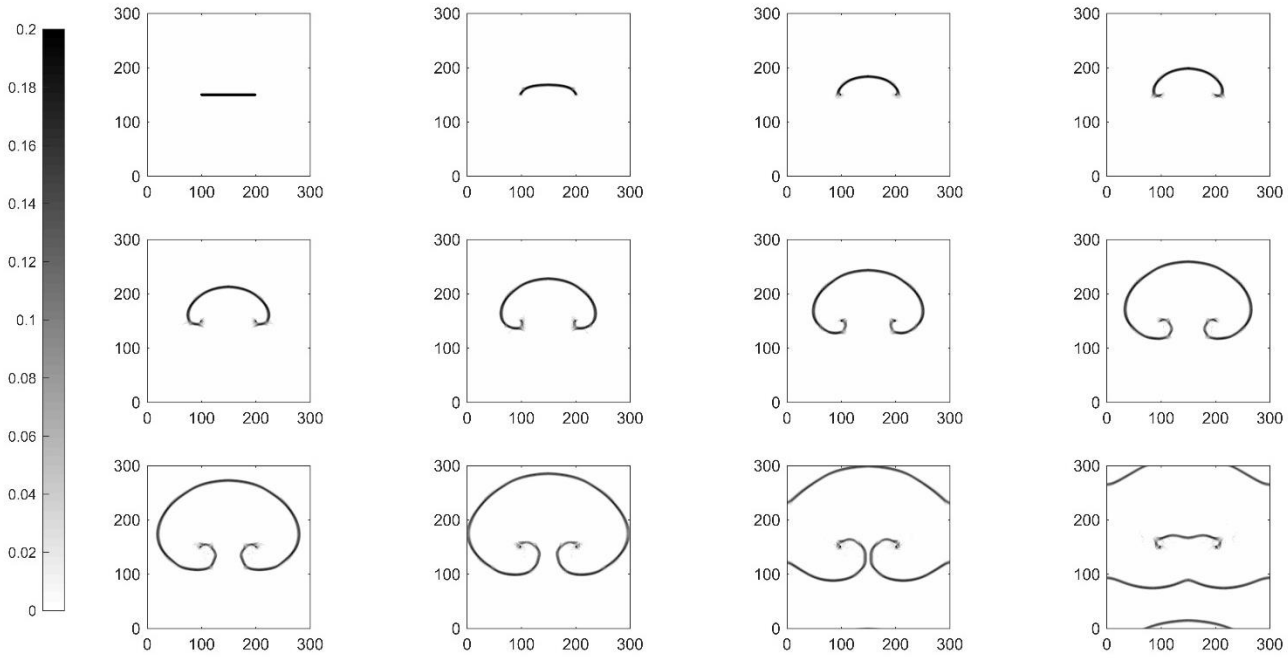

Fig. 11. The evolution of the Frank-Read source under applied shear stress 0.016 μ.

4.2.3 Orowan looping

In the last example, we apply the model to simulate Orowan looping as happening in precipitation hardening by non-shearable particles. Fig. 12(a) shows a single, straight dislocation bypassing two identical spherical obstacles in a periodic simulation cell, exhibiting the classical phenomenon of bow out, annihilation, pinch off, and finally leaving two dislocation loops surrounding the particles. Fig. 12(b) shows three straight dislocations moving in a precipitate field of 16 random obstacles. The dislocations bow out on meeting the obstacles and in this case, since the applied stress is not large enough, the dislocations stop moving in their bowed out configurations without by-passing. Fig. 12(c) shows another case of 9 random obstacles with dislocations bypassing them.

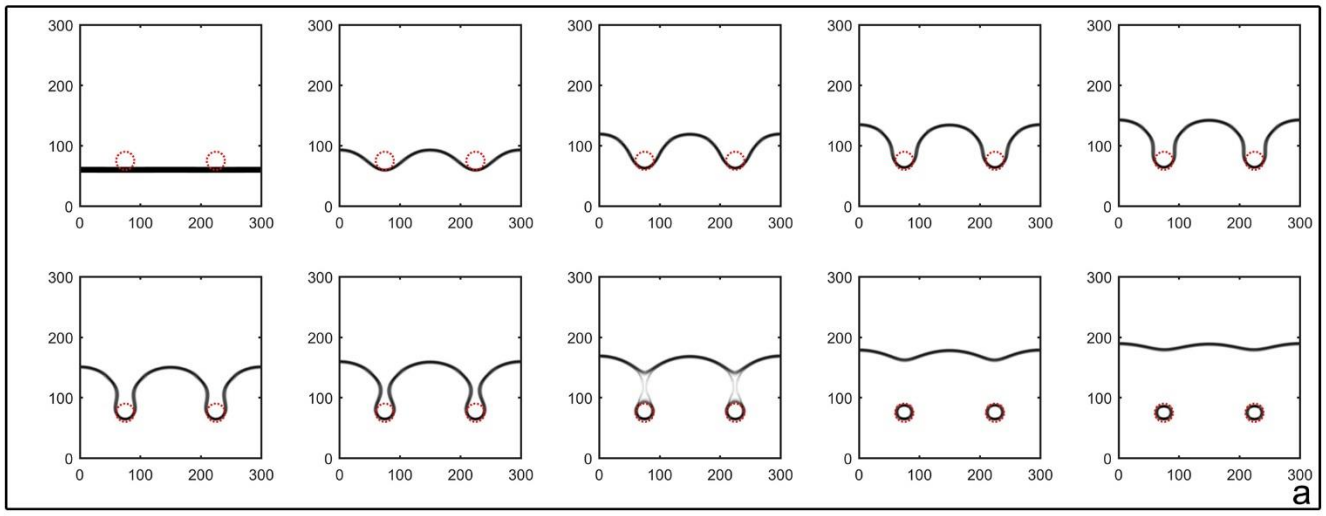
a

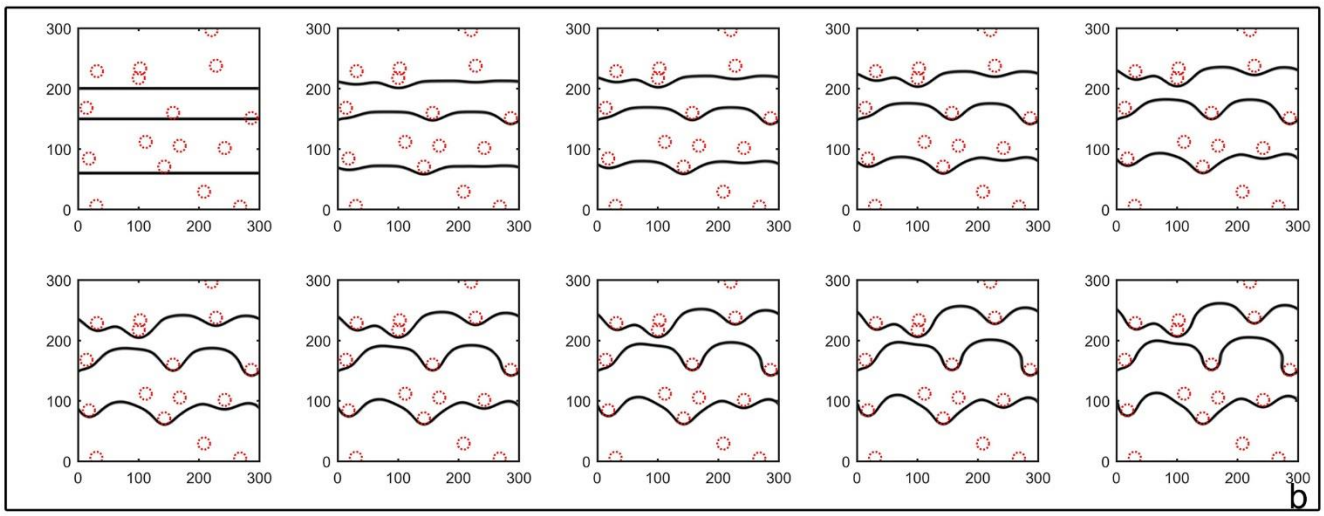
b

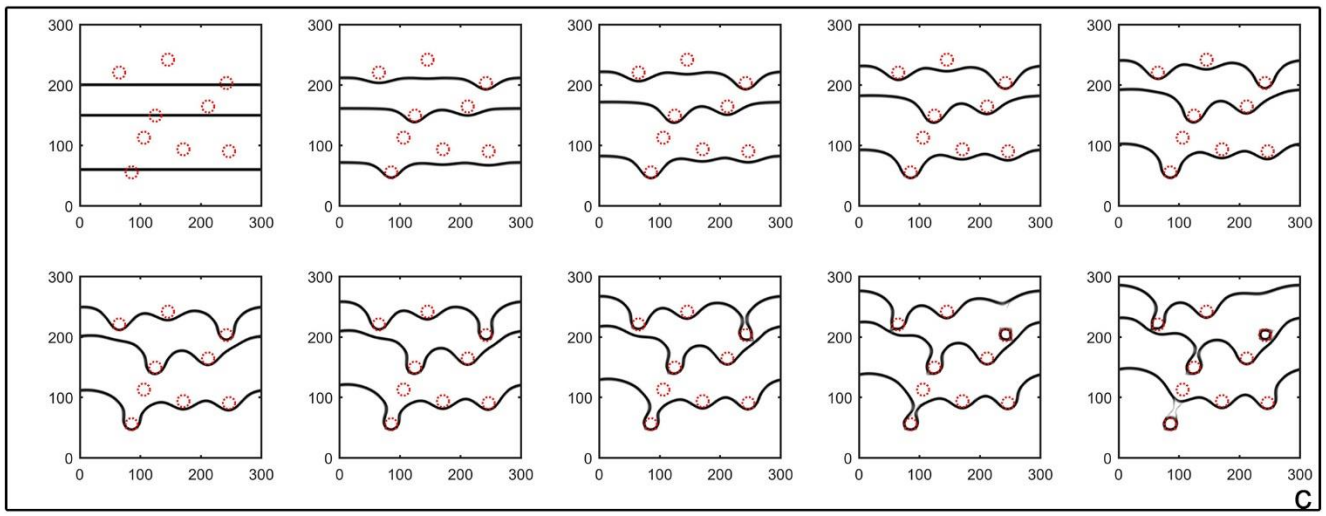
c

Fig. 12. (a) A single, initially straight dislocation bypassing two identical spherical obstacles in a periodic simulation cell, and leaving behind two dislocation loops around the particles at applied shear stress 0.031 μ. (b) Three initially straight dislocations moving in a precipitate field comprising 16 random obstacles, at applied shear stress 0.031 μ, getting immobilized eventually. (c) Three initially straight dislocations bypassing a precipitate field comprising 9 random obstacle, at applied shear stress 0.031 μ. The obstacles are drawn as red dot lines.

5. Discussion

5.1 Novelty statement

In the present work, a new framework is developed for modeling the dynamics of "intensive" dislocations. The main novelty of this framework lies on the consideration of dynamics to an extent not available before. First, elastic interactions are fully taken into account using the Mura formula. In particular, a special strategy for removing the singularity involved in Mura's integration kernel is used, to address the fact that the singularity is indeed forbidden in the "intensive" picture, in which any two spatial points on which the dislocation density can be defined meaningfully cannot be closer than the atomic resolution.

Secondly, a novel core-interaction function $f(d)$ is used to model the elastic and lattice-misfit interactions within the dislocation core. The traditional way to introduce a misfit stress from the γ-surface is not only computationally intractable in large systems, but also would not automatically give rise to a Peierls stress, which is a key aim of an "intensive" model of dislocations. The Peierls stress arises from fluctuations of the energy of the dislocation with respect to its position, and for a core description based on the γ-surface, the dislocation energy is the sum of the strain energy E_{strain} and the misfit energy E_{misfit}.

For a dislocation core at equilibrium, the Foreman-Nabarro theorem (Nabarro, 1947) states that the misfit energy, if calculated in a continuum manner as

$$E_{\text{misfit}} = \iint_{\text{slip plane}} \gamma(\mathbf{u}(\mathbf{x}))d^2x, \tag{44}$$

would always be an invariant quantity of $\mu b^2/(4\pi)$, regardless of the position of the dislocation (Hirth and Lothe, 1982) or its core shape (Ngan, 1997). In such a picture involving the γ-surface, the Peierls stress can therefore arise only from the fluctuations in the strain energy. For dislocations with a non-planar core, such fluctuations would arise from the required change in the core shape to a planar configuration as the dislocation begins to move (Ngan, 1997), but for dislocations with a planar core, there would be no provision for such a change in the core shape as the dislocation begins to move in the continuum γ-surface picture. One way to generate a non-zero Peierls stress from this continuum γ-surface picture would be to follow Peierls and Nabarro's approach to replace the integration in eqn. (44) by a summation over discrete lattice points on the slip plane (Hirth and Lothe, 1982), but this would be an extra, artificial step in a modelling strategy that is purely continuum. Another way to obtain a reasonable Peierls stress is to include an extra energy term that describes the interaction of the applied stress and discrete displacement in a semi-discrete variational approach (Bulatov and Kaxiras, 1997; Wei and Xiang, 2009). The present simulation strategy avoids using the γ-surface directly, which is computationally intractable anyway, and applies the factor $f(d)$ to mediate the elastic interaction within the core (eqns. (25) and (26)), which is what the γ-surface would serve to do. This achieves the two important functions of stabilizing the width of the dislocation as it moves, as well as automatically generating a resistance stress that mimics the Peierls stress. As is shown in Fig. 8, the core-width stabilizing function of the $f(d)$ factor results in a change in core shape as an external stress is applied and a critical stress needed to move the core, and neither of both would be achievable in a modeling strategy that is based on the continuum γ-surface picture; in that case

the core would simply move rigidly without any resistance, unless one is applied artificially to the simulation. Both the core width and the Peierls stress can be adjusted by the function $f(d)$, and so although this method is phenomenological, it is connectable to lower-level models such as molecular dynamics models that may provide core characteristics and Peierls stress directly. As mentioned, this method is computationally much more efficient than that involving the γ-surface directly, and if it is desirable to see what γ-surface a given $f(d)$ function would correspond to, we have shown in Section 4.1 that this can be done, by calculating the equilibrium density distribution for straight dislocations. In the example given in Section 4.1, the dislocation characters of purely edge and screw were simulated, giving the cross sections of the γ-surface along these two orientations, and the same process can be repeated for any dislocation character to give enough cross sections to generate the entire γ-surface. This way, our proposed method can be brought into full consistency with γ-surface approaches; for example, if the γ-surface of a given material is available from atomistic simulations, then the above strategy can be used to identify the best $f(d)$ function that would yield the closest γ-surface.

Finally, in this work, we demonstrate that a divergence-free numerical method is an effective tool to implement the evolution law of the dislocation density that can preserve the continuity from the initial condition well. Usual discrete numerical methods such as finite volume or finite element can normally conserve mass but divergence, and so if these methods are used to model dislocation density evolution, special strategies need to be devised in order to preserve the divergence (Varadhan et al., 2006).

5.2 Comparison with other approaches

It is worthwhile to compare the present model with others. First, although the classical Peierls-Nabarro model (Hirth and Lothe, 1982; Peierls, 1940) deals only with straight dislocations, Schoeck

generalized it for circular dislocation loops with a core shape that is independent of the circumferential location on the loop (Schoeck, 1995). Our approach, however, is capable of modeling 2D dislocation curves of any shape. Secondly, a number of authors have incorporated the γ-surface into phase field methods for modeling dislocation cores (Lee et al., 2011). The γ-surface is in the form of energy which is easily implemented in phase-field models that are energy-driven methods cast in the domain of lattice disregistry. As mentioned above, in this work we aim at developing a force-driven model making use of dislocation density as variable, and a lot of computation would be needed to convert dislocation density into disregistry (Roy and Acharya, 2005). Despite that the γ-surface is not directly used here, the core structures and properties shown in the present simulation results demonstrate that our model is capable of describing the dislocation interaction in a rather straightforward way. Also, these phase-field methods fail to model the Peierls stress. "Intensive" descriptions of dislocations have also been made via atomistic/continuum coupling models such as the bridging domain method with extended finite element method (XFEM-BDM) (Gracie and Belytschko, 2011, 2009), coupled atomistic and discrete dislocation plasticity (CADD) (Curtin and Miller, 2003; Shilkrot et al., 2002) and the concurrent atomistic–continuum (CAC) methodology (Xiong et al., 2015, 2012). Although these directly coupled multi-scale models are elegant, their complexity are much higher than the present framework and the coupling process may induce numerically instability while this is not a problem in the present approach based on continuum mechanics.

5.3 Limitations and future work

In the present model, the density distribution for a given slip system is assumed to have the same Burgers vector. While this has to be the case in the "extensive" and "discrete" representations, in the "intensive" representation this would forbid core dissociation into partials with slightly different partial

Burgers vectors. For instance, the classical Escaig constriction phenomenon (Liu et al., 2017) relies on the partial dislocations exhibiting a small dipole character, so that a given resolved shear stress can constrict the dislocation core to assist cross-slip or climb. In the present model, the external stress has no effect on the core width all the dislocation densities in the core possess the same Burgers vector. To solve this problem, a formalism based on the Nye tensor $\boldsymbol{\alpha}$ instead of the dislocation density vector $\boldsymbol{\rho}$ with constant Burgers vector $\mathbf{b}$ would allow the Burgers vector to be represented as a variable $\mathbf{b}(\mathbf{x})$. The major problem to implement the Nye tensor, however, concerns the velocity law (Acharya et al., 2006). The velocity field is a function of the Peach-Koehler force $\mathbf{F}^{\mathrm{PK}} = \boldsymbol{\sigma} \cdot \mathbf{b} \times \boldsymbol{\rho}/\|\boldsymbol{\rho}\|$, and so without detailed information on $\boldsymbol{\rho}(\mathbf{x})$ and $\mathbf{b}(\mathbf{x})$, simply knowing the Nye tensor $\boldsymbol{\alpha}(\mathbf{x})$ alone would not allow the Peach-Koehler force or the velocity to be uniquely obtained. Instead, a better approach would be to use a separate density function $\boldsymbol{\rho_i}$ for each specific Burgers vector $\mathbf{b_i}$ allowable in the system. The problem becomes solving a system of simultaneous equations, one for each $\boldsymbol{\rho_i}$, but since the number of the allowable $\mathbf{b_i}$ is not large, this will not be a serious problem. There will be interactions between the different $\boldsymbol{\rho_i}$ but these, such as the elastic interactions, can still be handled using the present framework. Future work may focus on such an approach.

Secondly, it would not be feasible to scale up directly from the present framework of slip on a plane to treat multiple slips on intersecting systems. To do this, the framework would need to include consideration of cross-slip, climb and dislocation junctions. Modifying the velocity law to include thermal activation effects can handle climb and cross-slip, but modeling dislocation junctions in the "intensive" picture would need a very special core interaction function. Even if models for all these mechanisms are available, the computational time for a 3-D calculation of a large system in the "intensive" representation would be enormous. Therefore, although it is possible to improve the present framework for large 3-D systems, developing better "extensive" models would be the more realistic way forward.

6. Conclusions

In the present study, a novel dislocation-density based framework for the "intensive" representation of dislocations is proposed. To handle dislocation cores at such a resolution scale, both inter-dislocation elastic interaction and interactions within dislocation cores are modeled. For core interactions, a special representation of the lattice misfit interaction is proposed to counteract the elastic interaction, which serves not only to maintain the width of the dislocation as it glides, but also to generate a Peierls stress. A divergence preserving numerical method is used to solve the dynamics evolution law for the dislocation densities. Simulation examples including loop shrinkage and expansion, the Frank-Read sources, and Orowan looping demonstrate excellent preservation of the continuity of the dislocation density, as well as clear elucidation of the details of the core structure as the dislocations glide.

Acknowledgement

The work reported here was supported by the Kingboard Professorship in Materials Engineering at the University of Hong Kong.

References

Acharya, A., Roy, A., 2006. Size effects and idealized dislocation microstructure at small scales: Predictions of a Phenomenological model of Mesoscopic Field Dislocation Mechanics: Part I. J. Mech. Phys. Solids 54, 1687–1710.

Acharya, A., Roy, A., Acharya, A., Roy, A., Acharya, A., 2006. Size effects and idealized dislocation microstructure at small scales: Predictions of a Phenomenological model of Mesoscopic Field

Dislocation Mechanics: Part II. J. Mech. Phys. Solids 54, 1711–1743. https://doi.org/10.1016/j.jmps.2006.01.012

Arsenlis, A., Parks, D.M., 2002. Modeling the evolution of crystallographic dislocation density in crystal plasticity. J. Mech. Phys. Solids 50, 1979–2009. https://doi.org/10.1016/S0022-5096(01)00134-X

Arsenlis, A., Parks, D.M., Becker, R., Bulatov, V. V., 2004. On the evolution of crystallographic dislocation density in non-homogeneously deforming crystals. J. Mech. Phys. Solids 52, 1213–1246. https://doi.org/10.1016/j.jmps.2003.12.007

Artebrant, R., Torrilhon, M., 2008. Increasing the accuracy in locally divergence-preserving finite volume schemes for MHD. J. Comput. Phys. 227, 3405–3427. https://doi.org/10.1016/j.jcp.2007.12.003

Banerjee, S., Ghoniem, N., Lu, G., Kioussis, N., 2007. Non-singular descriptions of dislocation cores: a hybrid *ab initio* continuum approach. Philos. Mag. 87, 4131–4150. https://doi.org/10.1080/14786430701528739

Benoit, W., Bujard, M., Germaud, G., 1987. Kink dynanmics in FCC metals. Phys. status solidi 104, 427–441.

Bulatov, V., Cai, W., Fier, J., Hiratani, M., Hommes, G., Pierce, T., Tang, M., Rhee, M., Yates, K., Arsenlis, T., 2004. Scalable Line Dynamics in ParaDiS, in: Proceedings of the 2004 ACM/IEEE Conference on Supercomputing, SC '04. IEEE Computer Society, Washington, DC, USA, p. 19--. https://doi.org/10.1109/SC.2004.53

Bulatov, V. V., Kaxiras, E., 1997. Semidiscrete Variational Peierls Framework for Dislocation Core Properties. Phys. Rev. Lett. 78, 4221–4224. https://doi.org/10.1103/PhysRevLett.78.4221

Bulatov, V. V, Hsiung, L.L., Tang, M., Arsenlis, A., Bartelt, M.C., Cai, W., Florando, J.N., Hiratani, M., Rhee, M., Hommes, G., Pierce, T.G., de la Rubia, T.D., 2006. Dislocation multi-junctions and strain hardening. Nature 440, 1174–1178. https://doi.org/10.1038/nature04658

Bullough, B. and Tewary, V.K., 1979. Lattice theories of dislocations: in F.R.N. Nabarro (ed), Dislocations in Solids, North-Holland, Amsterdam, Vol. 2, Ch. 5.

Cai, W., Arsenlis, A., Weinberger, C.R., Bulatov, V. V., 2006. A non-singular continuum theory of dislocations. J. Mech. Phys. Solids 54, 561–587. https://doi.org/10.1016/j.jmps.2005.09.005

Christian, J.W., Vítek, V., 1970. Dislocations and stacking faults. Reports Prog. Phys. 33, 307. https://doi.org/10.1088/0034-4885/33/1/307

Curtin, W. a, Miller, R.E., 2003. Atomistic / continuum coupling in computational materials science. Model. Simul. Mater. Sci. Eng. 11, R33–R68. https://doi.org/10.1088/0965-0393/11/3/201

Dai, F.Z., Zhang, W.Z., 2015. An automatic and simple method for specifying dislocation features in atomistic simulations. Comput. Phys. Commun. 188, 103–109. https://doi.org/10.1016/j.cpc.2014.11.014

Engels, P., Ma, A., Hartmaier, A., 2012. Continuum simulation of the evolution of dislocation densities during nanoindentation. Int. J. Plast. 38, 159–169. https://doi.org/10.1016/j.ijplas.2012.05.010

Gbemou, K., Taupin, V., Raulot, J.M., Fressengeas, C., 2016. Building compact dislocation cores in an elasto-plastic model of dislocation fields. Int. J. Plast. 82, 241–259. https://doi.org/10.1016/j.ijplas.2016.03.007

Gracie, R., Belytschko, T., 2011. An adaptive concurrent multiscale method for the dynamic simulation of dislocations. Int. J. Numer. Methods Eng. 86, 575–597. https://doi.org/10.1002/nme.3112

Gracie, R., Belytschko, T., 2009. Concurrently coupled atomistic and XFEM models for dislocations and cracks. Int. J. Numer. Methods Eng. 78, 354–378. https://doi.org/10.1002/nme.2488

Groma, I., Csikor, F.F., Zaiser, M., 2003. Spatial correlations and higher-order gradient terms in a continuum description of dislocation dynamics. Acta Mater. 51, 1271–1281. https://doi.org/10.1016/S1359-6454(02)00517-7

Groma, I., Zaiser, M., Ispánovity, P.D., 2016. Dislocation patterning in a two-dimensional continuum theory of dislocations. Phys. Rev. B 93. https://doi.org/10.1103/PhysRevB.93.214110

Hirth, J.P., Lothe, J., 1982. Theory of dislocations, second ed, Krieger Publishing Company, Malabar, Florida.

Hochrainer, T., Sandfeld, S., Zaiser, M., Gumbsch, P., 2014. Continuum dislocation dynamics: Towards a physical theory of crystal plasticity. J. Mech. Phys. Solids 63, 167–178. https://doi.org/10.1016/j.jmps.2013.09.012

Hochrainer, T., Zaiser, M., Gumbsch, P., 2007. A three-dimensional continuum theory of dislocation systems: kinematics and mean-field formulation. Philos. Mag. 87, 1261–1282. https://doi.org/10.1080/14786430600930218

Höllerbauer, W., Karnthaler, H.P., 1981. Beitr. elektonenmicr. Direktabb. Oberfl 14, 361.

Jamond, O., Gatti, R., Roos, A., Devincre, B., 2016. Consistent formulation for the Discrete-Continuous Model: Improving complex dislocation dynamics simulations. Int. J. Plast. 80, 19–37. https://doi.org/10.1016/j.ijplas.2015.12.011

Koslowski, M., Cuitiño, A.M., Ortiz, M., 2002. A phase-field theory of dislocation dynamics, strain hardening and hysteresis in ductile single crystals. J. Mech. Phys. Solids 50, 2597–2635.

https://doi.org/10.1016/S0022-5096(02)00037-6

Kröner, E., 1958. Kontinuumstheorie der versetzungen und eigenspannungen. Springer.

Lee, D.W., Kim, H., Strachan, A., Koslowski, M., 2011. Effect of core energy on mobility in a continuum dislocation model. Phys. Rev. B - Condens. Matter Mater. Phys. 83, 1–10. https://doi.org/10.1103/PhysRevB.83.104101

LeSar, R., 2014. Simulations of Dislocation Structure and Response. Annu. Rev. Condens. Matter Phys. 5, 375–407. https://doi.org/10.1146/annurev-conmatphys-031113-133858

Leung, H.S., Leung, P.S.S., Cheng, B., Ngan, A.H.W., 2015. A new dislocation-density-function dynamics scheme for computational crystal plasticity by explicit consideration of dislocation elastic interactions. Int. J. Plast. 67, 1–25. https://doi.org/10.1016/j.ijplas.2014.09.009

Leung, H.S., Ngan, A.H.W., 2016. Dislocation-density function dynamics - An all-dislocation, full-dynamics approach for modeling intensive dislocation structures. J. Mech. Phys. Solids 91, 172–203. https://doi.org/10.1016/j.jmps.2016.03.008

Li, D., Zbib, H., Sun, X., Khaleel, M., 2014. Predicting plastic flow and irradiation hardening of iron single crystal with mechanism-based continuum dislocation dynamics. Int. J. Plast. 52, 3–17. https://doi.org/10.1016/j.ijplas.2013.01.015

Liu, G., Cheng, X., Wang, J., Chen, K., Shen, Y., 2017. Quasi-periodic variation of Peierls stress of dislocations in face-centered-cubic metals. Int. J. Plast. 90, 156–166. https://doi.org/10.1016/j.ijplas.2017.01.002

Lu, G., Kioussis, N., Bulatov, V. V., Kaxiras, E., 2000. Generalized-stacking-fault energy surface and dislocation properties of aluminum. Phys. Rev. B 62, 3099–3108.

https://doi.org/10.1103/PhysRevB.62.3099

Martínez, E., Marian, J., Arsenlis, A., Victoria, M., Perlado, J.M., 2008. Atomistically informed dislocation dynamics in fcc crystals. J. Mech. Phys. Solids 56, 869–895. https://doi.org/10.1016/j.jmps.2007.06.014

Mishra, S., Tadmor, E., 2010. Constraint Preserving Schemes Using Potential-Based Fluxes I. Multidimensional Transport Equations. Commun. Comput. Phys. 9, 688–710. https://doi.org/10.4208/cicp.030909.091109s

Mura, T., 2013. Micromechanics of defects in solids. Springer Science & Business Media.

Nabarro, F.R.N., 1997. Theoretical and experimental estimates of the Peierls stress. Philos. Mag. A 75, 703–711. https://doi.org/10.1080/01418619708207197

Nabarro, F.R.N., 1947. Dislocations in a simple cubic lattice. Proc. Phys. Soc. 59, 256.

Ngan, A.H., 1995. A critique on some of the concepts regarding planar faults in crystals. Philos. Mag. Lett. 72, 11–19. https://doi.org/10.1080/09500839508241609

Ngan, A.H.W., 2017. Dislocation-density kinematics: a simple evolution equation for dislocation density involving movement and tilting of dislocations. MRS Commun. 1–8. https://doi.org/10.1557/mrc.2017.66

Ngan, A.H.W., 1997. A generalized Peierls-Nabarro model for nonplanar screw dislocation cores. J. Mech. Phys. Solids 45, 903–921. https://doi.org/10.1016/S0022-5096(96)00125-1

Nye, J.F., 1953. Some geometrical relations in dislocated crystals. Acta Metall. 1, 153–162.

Peierls, R., 1940. The size of a dislocation. Proc. Phys. Soc. 52, 34–37. https://doi.org/10.1088/0959-5309/52/1/305

Po, G., Lazar, M., Admal, N.C., Ghoniem, N., 2017. A non-singular theory of dislocations in anisotropic crystals. Int. J. Plast. https://doi.org/10.1016/j.ijplas.2017.10.003

Roy, A., Acharya, A., 2005. Finite element approximation of field dislocation mechanics. J. Mech. Phys. Solids 53, 143–170. https://doi.org/10.1016/j.jmps.2004.05.007

Sandfeld, S., Thawinan, E., Wieners, C., 2015. A link between microstructure evolution and macroscopic response in elasto-plasticity: Formulation and numerical approximation of the higher-dimensional continuum dislocation dynamics theory. Int. J. Plast. 72, 1–20. https://doi.org/10.1016/j.ijplas.2015.05.001

Schoeck, G., 1995. The Peierls model for dislocation rings. Czechoslov. J. Phys. 45, 991–1002. https://doi.org/10.1007/BF01692015

Seeger, A., Schiller, P., Mason, W.P., Thurston, R.N., 1966. Physical Acoustics, Vol. IIIA. Acad. New York 361.

Shilkrot, L.E., Miller, R.E., Curtin, W.A., 2002. Coupled Atomistic and Discrete Dislocation Plasticity. Phys. Rev. Lett. 89, 25501. https://doi.org/10.1103/PhysRevLett.89.025501

Shin, I., Carter, E.A., 2013. Possible origin of the discrepancy in Peierls stresses of fcc metals: First-principles simulations of dislocation mobility in aluminum. Phys. Rev. B - Condens. Matter Mater. Phys. 88, 1–10. https://doi.org/10.1103/PhysRevB.88.064106

Torrilhon, M., 2005. Locally divergence-preserving upwind finite volume schemes for magnetohydrodynamic equations. SIAM J. Sci. Comput. 26, 1166–1191. https://doi.org/10.1137/S1064827503426401

Varadhan, S.N., Beaudoin, A.J., Acharya, A., Fressengeas, C., 2006. Dislocation transport using an

explicit Galerkin/least-squares formulation. Model. Simul. Mater. Sci. Eng. 14, 1245–1270. https://doi.org/10.1088/0965-0393/14/7/011

Vítek, V., Kroupa, F., 1969. Generalized splitting of dislocations. Philos. Mag. 19, 265–284. https://doi.org/10.1080/14786436908217784

Wang, Y.U., Jin, Y.M., Cuitiño, A.M., Khachaturyan, A.G., 2001. Nanoscale phase field microelasticity theory of dislocations: Model and 3D simulations. Acta Mater. 49, 1847–1857. https://doi.org/10.1016/S1359-6454(01)00075-1

Wei, H., Xiang, Y., 2009. A generalized Peierls-Nabarro model for kinked dislocations. Philos. Mag. 89, 2333–2354. https://doi.org/10.1080/14786430903103968

Woodward, C., Trinkle, D.R., Hector, L.G., Olmsted, D.L., 2008. Prediction of dislocation cores in aluminum from density functional theory. Phys. Rev. Lett. 100, 1–4. https://doi.org/10.1103/PhysRevLett.100.045507

Xiang, Y., Cheng, L.-T., Srolovitz, D.J., E, W., 2003. A level set method for dislocation dynamics. Acta Mater. 51, 5499–5518. https://doi.org/10.1016/S1359-6454(03)00415-4

Xiang, Y., Wei, H., Ming, P., E, W., 2008. A generalized Peierls-Nabarro model for curved dislocations and core structures of dislocation loops in Al and Cu. Acta Mater. 56, 1447–1460. https://doi.org/10.1016/j.actamat.2007.11.033

Xiong, L., Deng, Q., Tucker, G., McDowell, D.L., Chen, Y., 2012. A concurrent scheme for passing dislocations from atomistic to continuum domains. Acta Mater. 60, 899–913. https://doi.org/10.1016/j.actamat.2011.11.002

Xiong, L., Xu, S., McDowell, D.L., Chen, Y., 2015. Concurrent atomistic-continuum simulations of

dislocation-void interactions in fcc crystals. Int. J. Plast. 65, 33–42. https://doi.org/10.1016/j.ijplas.2014.08.002

Zhu, Y., Wang, H., Zhu, X., Xiang, Y., 2014. A continuum model for dislocation dynamics incorporating Frank-Read sources and Hall-Petch relation in two dimensions. Int. J. Plast. 60, 19–39. https://doi.org/10.1016/j.ijplas.2014.04.013

Appendix

A. Solving displacement field from Nye tensor

Let $\mathbf{u}(\mathbf{x})$ be the displacement field of the crystal as the dislocation densities under consideration are introduced into it, and $\mathbf{x}$ denotes the coordinates in the initial crystal. Under the displacement field described by $\mathbf{u}(\mathbf{x})$, an infinitesimally short vector $d\mathbf{x}$ starting from point $\mathbf{x}$ in the initial state is mapped into the vector $d\mathbf{x}'$ in the deformed state which is given by:

$$d\mathbf{x}' = (\mathbf{x} + d\mathbf{x} + \mathbf{u} + d\mathbf{u}) - (\mathbf{x} + \mathbf{u}) = d\mathbf{x} + d\mathbf{u} \tag{A1.1}$$

However, $du_i = \left(u_{i,j}dx_j\right)$, in a vector form $d\mathbf{u} = d\mathbf{x} \cdot (\boldsymbol{\nabla}\otimes\mathbf{u})$ and so (A1) becomes $d\mathbf{x}' = d\mathbf{x} \cdot \mathbf{G}$, where

$$\mathbf{G} = \left(\mathbf{I} + (\boldsymbol{\nabla}\otimes\mathbf{u})\right) \tag{A1.2}$$

is the deformation tensor linking the initial vector $d\mathbf{x}$ to the deformed vector $d\mathbf{x}'$, and $\mathbf{I}$ is the identity tensor. The Nye tensor is defined in terms of $\mathbf{G}$ by $\boldsymbol{\alpha} = -\boldsymbol{\nabla} \times \mathbf{G}$ (Dai and Zhang, 2015; Kröner, 1958), and hence

$$\boldsymbol{\alpha} = -\boldsymbol{\nabla} \times \left(\mathbf{I} + (\boldsymbol{\nabla}\otimes\mathbf{u})\right) = -\boldsymbol{\nabla} \times (\boldsymbol{\nabla}\otimes\mathbf{u}) \tag{A1.3}$$

B. Comparison with Discrete Dislocation Dynamics (DDD) simulations

DDD simulations were performed using the ParaDis code (Bulatov et al., 2004). It should be noted that in the present ParaDis code, there is no description of the core interaction other than the removal of the elastic stress singularity via eqn. (15), and the line discretization method used is quite different from the present spatial discretization of dislocation density; there is therefore no good reason to expect full agreement between the DDD predictions and those from the present model. Fig. 13 shows the DDD prediction of loop expansion and shrinkage from an initial circular loop, and the results here match rather well with Fig. 10 from the present model. Since the Peierls stress is not used in the DDD method, we used different mobility for screw and edge dislocations in a ratio of 2:3. Fig. 14 shows the DDD prediction of the operation of a Frank-Read source under an applied shear stress of 0.048 μ, which is higher than the 0.016 μ in Fig. 11. The operating stress of a Frank-Read source is expected to be $\mu b/L$ where L is the length of the source, which is set to be 100 b. Therefore, the source is expected to operate at 0.01μ, which is close to the stress in Fig. 11. In the DDD simulation shown in Fig. 14, the initial dislocation segment does begin to move at 0.01μ but it fails to evolve further to achieve a pinch-off configuration. The much higher stress needed to fully operate the source in the DDD is due to a very low rotational ability of the free ends, which may be caused by the rather long discretization length of the dislocation in the range of 3.5-10 b, while the simulation pixel is much smaller at 1 b ×1 b in our density framework in Fig. 11. The long discretized length in the DDD may not be accurate enough for the high curvature of the dislocation at the two free ends.

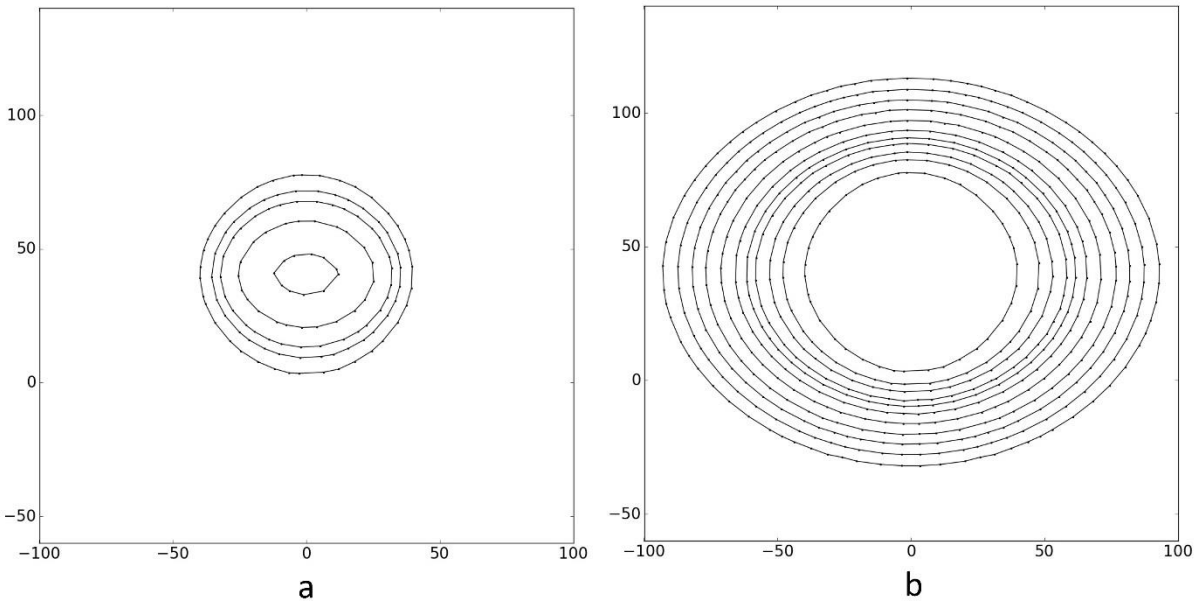

Fig. 13. Results from DDD solver. (a) Shrinkage of a single loop under self stress, and (b) expansion of a loop under an applied shear stress 0.0308 μ. The initial loop for both situations is the same which is the largest one in the shrinkage case and the smallest one in the expansion case. Screw direction is horizontal in both cases.

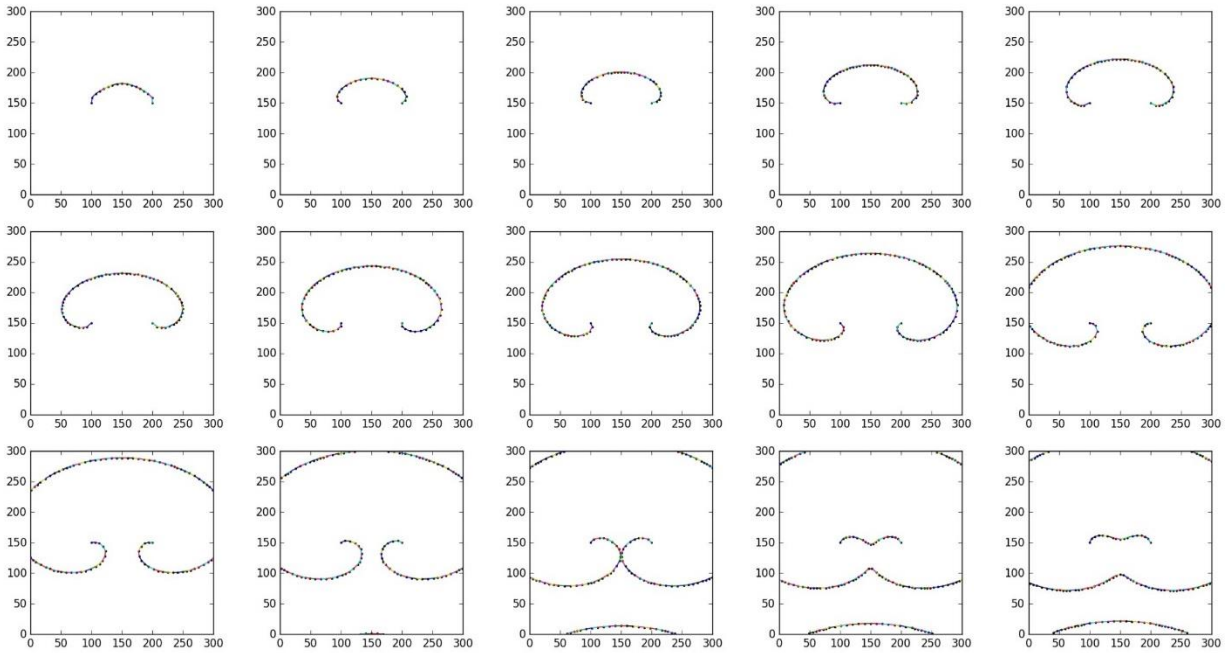

Fig. 14. Evolution of Frank-Read source under applied shear stress 0.048 μ as predicted by DDD solver.